

## NORA3. Part II: Precipitation and Temperature Statistics in Complex Terrain Modeled with a Nonhydrostatic Model

HILDE HAAKENSTAD<sup>a,b</sup> AND ØYVIND BREIVIK<sup>a,b</sup>

<sup>a</sup> Norwegian Meteorological Institute, Oslo, Norway

<sup>b</sup> Geophysical Institute, University of Bergen, Bergen, Norway

(Manuscript received 31 January 2022, in final form 1 July 2022)

**ABSTRACT:** The 3-km Norwegian Reanalysis (NORA3) is a convection-permitting, nonhydrostatic hindcast for the North Sea, the Norwegian Sea, and the Barents Sea as well as the Scandinavian Peninsula. It has a horizontal resolution of 3 km and provides a full three-dimensional atmospheric state for the period 1995–2020 with a surface analysis and boundary conditions from ERA5, a global reanalysis. In complex terrain it is found to outperform both the host reanalysis ERA5 and also the earlier hydrostatic 10-km Norwegian Hindcast Archive (NORA10), in terms of 2-m temperature and daily precipitation. Of particular interest is the representation of extreme rainfall. It is found that the upper percentiles are much better represented than in ERA5, with very little bias up to 99.9%, suggesting that the new hindcast archive is well suited for hydrological mapping and extreme-value analysis of rainfall in complex terrain.

**SIGNIFICANCE STATEMENT:** High-resolution hindcasts that permit realistic convection allow very detailed modeling of the surface temperature, precipitation, and wind field in complex terrain. There is a need for detailed mapping of rainfall and temperature extremes (upper percentiles) to assess the impact of rapid climate change. We present an assessment of the performance of the model from Part I for near-surface temperature and precipitation, which are found to be much improved in comparison with ERA5 and with earlier NORA10. The focus is on the Norwegian mainland and the Svalbard Archipelago, because the complex terrain found in these regions is challenging to represent in weather prediction models. The improvement in precipitation statistics is particularly pronounced, with nearly unbiased results up to the 99.9th percentile.

**KEYWORDS:** Arctic; Complex terrain; Precipitation; Reanalysis data; Surface temperature; Nonhydrostatic models

### 1. Introduction


Near-surface temperature and precipitation are meteorological variables that are strongly influenced by surface properties and topography. Precipitation also exhibits a strong response to the general warming that is mainly driven by anthropogenic forcing (IPCC 2007; Haarsma et al. 2013; Whan et al. 2020). The response amplifies through several feedback effects, which are particularly strong in the Arctic due to the more rapid climate change in these areas (Vihma et al. 2015). Modeling the precipitation and temperature climatology with high spatial and temporal resolution is thus important both to establish a baseline for trends in future projections and to assess the extremes of present-day climate. High-resolution precipitation fields are also essential in hydrological modeling of floods, landslides, and avalanches (Schaller et al. 2020).

Global reanalyses based on fixed numerical weather prediction models and a data assimilation system that ingests an (ideally) fixed set of observations represent the best large-scale reconstructions of past weather. However, their resolution is still far too coarse to resolve complex topography and in Arctic regions

they suffer from a scarcity of observations, even though this has improved with increased satellite information in the past decades (Bell et al. 2020; Horányi 2017).

Reanalyses are also expensive to run. Therefore, a common procedure is to downscale the reanalyses to properly resolve topographical features while forgoing a full assimilation of observations. Several downscalings have been produced for the North Sea region, where they have been used to assess marine wind and wave climate (Dörenkämper et al. 2020; Weisse and Günther 2007; Reistad et al. 2011; Aarnes et al. 2012; Haakenstad et al. 2020).

The 3-km Norwegian Reanalysis (NORA3; Haakenstad et al. 2021) is such a hindcast, as these downscalings are called when no assimilation of own observations is performed (note though that NORA3 contains a surface analysis scheme and thus technically falls somewhere between a full reanalysis and a hindcast). Here, the latest reanalysis from the European Centre for Medium-Range Weather Forecasts (ECMWF), ERA5 (Hersbach et al. 2020), is used as the host analysis for a downscaling with the nonhydrostatic convection-permitting (C-P) model HARMONIE-AROME (Seity et al. 2011; Bengtsson et al. 2017; Termonia et al. 2018). A C-P model resolves deep

 Denotes content that is immediately available upon publication as open access.

Corresponding author: Øyvind Breivik, oyvind.breivik@met.no



This article is licensed under a [Creative Commons Attribution 4.0 license](http://creativecommons.org/licenses/by/4.0/) (<http://creativecommons.org/licenses/by/4.0/>).

DOI: 10.1175/JAMC-D-22-0005.1

© 2022 American Meteorological Society. For information regarding reuse of this content and general copyright information, consult the [AMS Copyright Policy](#) ([www.ametsoc.org/PUBSReuseLicenses](http://www.ametsoc.org/PUBSReuseLicenses)).

## Station map for 2m temperature.

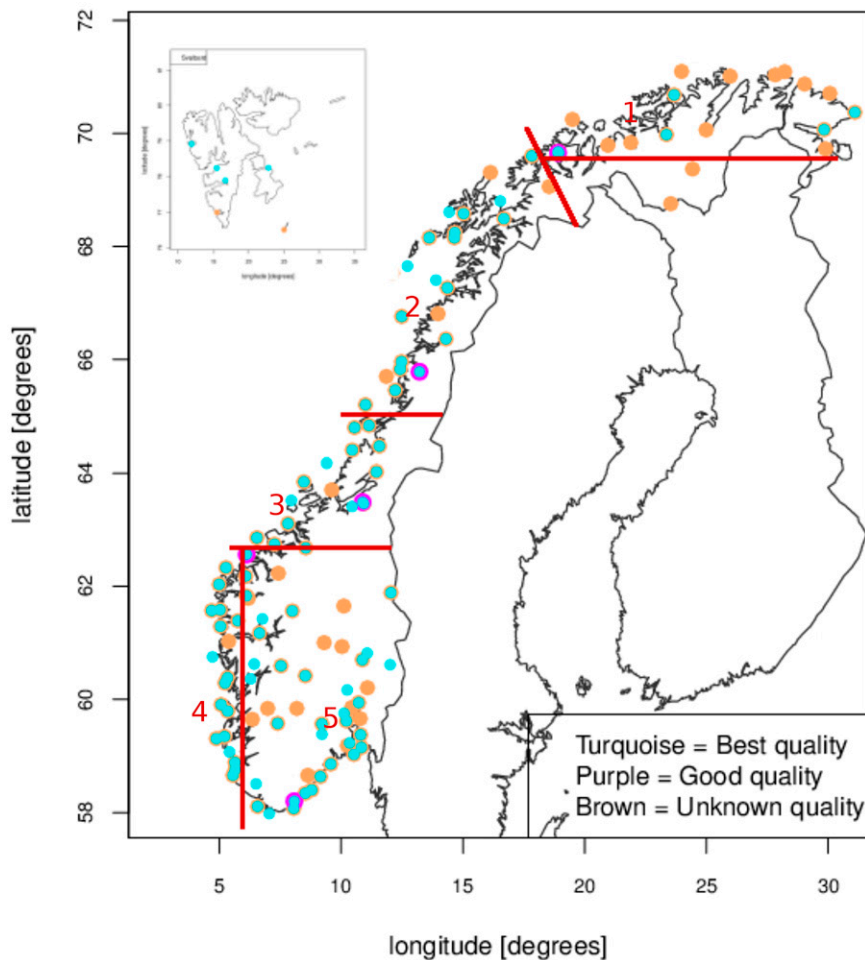


FIG. 1. Map showing the stations used in the 2-m temperature validation for the mainland and the Svalbard Archipelago (inset) and the quality level of the stations. Turquoise denotes quality 0 (the best quality), purple denotes quality 1 (good quality, but with a possibility that the values have been adjusted in the quality checks) and light brown marks observations of quality 2 (of unknown quality). The boundaries of the five regions of the Norwegian mainland used for the validation of the northeastern coast and northern inner area (area 1) counting 5 stations, the northern coastal area (area 2) with 23 stations, the middle area (area 3) counting 18 stations, the southwestern coast (area 4) counting 17 stations, and the southeastern area (5) with 34 stations are indicated with red lines.

convection and has a more realistic water cycle than do models using parameterized deep convection. Nonhydrostatic C-P models solve the fully compressible Euler equations. This yields realistic vertical accelerations, which by contrast are calculated diagnostically in hydrostatic models after assuming a balance between the pressure gradient force and the gravitational force. A nonhydrostatic C-P model with grid resolution of 2–3 km and sophisticated microphysics is expected to more realistically reproduce squall lines, thunderstorms, and orographically induced gravity waves. Such models will also tend to have more realistic fluxes of momentum, turbulent energy, heat and moisture between the surface and the atmosphere. The surface wind field of NORA3 was

investigated by [Haakenstad et al. \(2021\)](#). The topic of this article is the performance of NORA3 in terms of 2-m temperature and daily precipitation. In particular, we investigate whether a nonhydrostatic model constrained only by a surface analysis and frequent initializations based on a much coarser reanalysis (ERA5) is capable of resolving temperature gradients and rainfall in a region with highly complex terrain, namely the Norwegian mainland and the Svalbard Archipelago. The period from 1995 until the end of 2020 is considered here, but the hindcast is continuously updated to the present and will also in due time come to cover the period from 1979. The host reanalysis, ERA5 is described in [Hersbach et al. \(2020\)](#). ERA5 has a horizontal

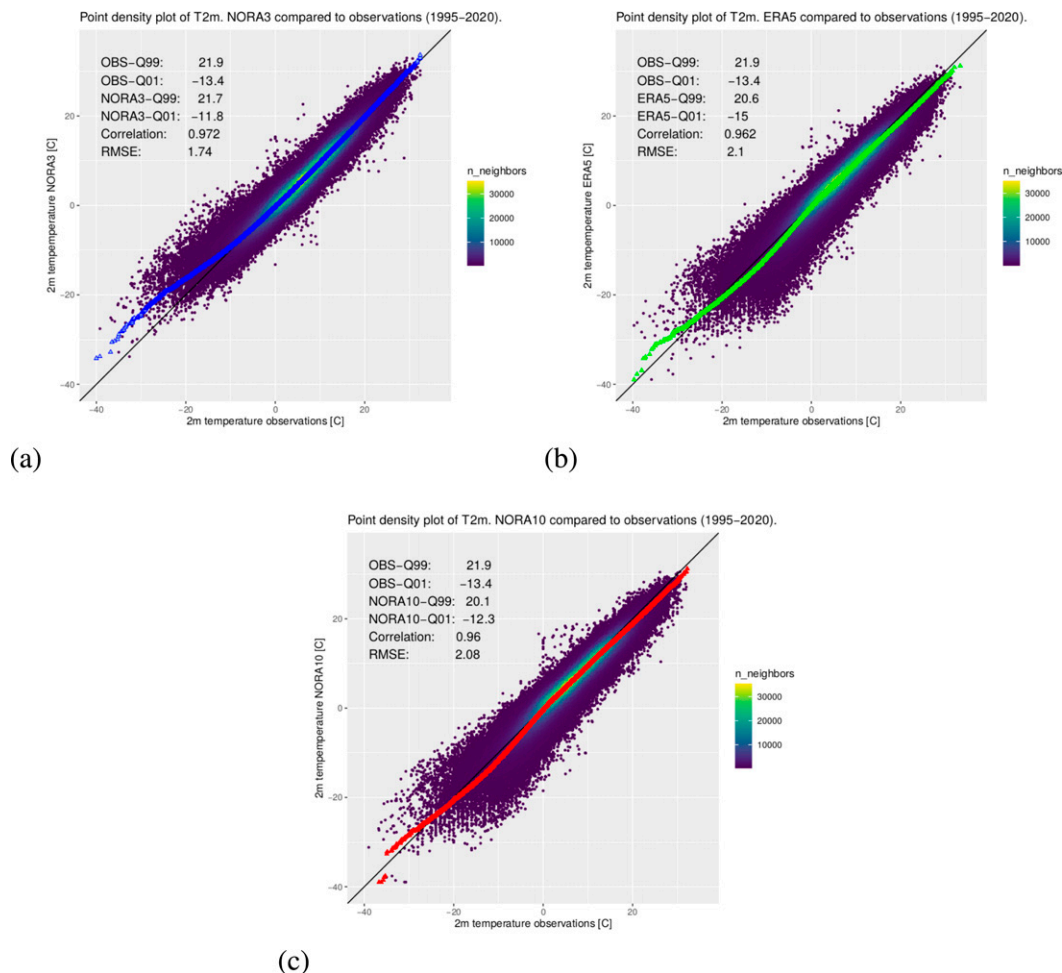


FIG. 2. Scatter density plot of T2m for (a) NORA3, (b) ERA5, and (c) NORA10. The percentiles 1 and 99, together with the correlation and RMSE are reported in the legend.

resolution of approximately 31 km and is produced with the Integrated Forecasting System (IFS) Cy41r2. A four-dimensional variational data assimilation system has been used in the production of ERA5 to achieve the best possible fit between the model and the observations over the whole analysis window. Two-way coupling between atmosphere and land and also between atmosphere and waves, exists in the production of ERA5. By contrast, NORA3 as a dynamically downscaled hindcast uses only a simple optimal interpolation scheme for the surface analysis and has no upper-air assimilation.

This article is organized as follows. In section 2 we briefly describe the numerical weather prediction model and the way it has been set up. This description is on purpose kept short since it has already been documented in part I of this work (Haakenstad et al. 2021). Section 3 presents the observation network used in this study while section 4 presents the main findings. Here we compare the performance of NORA3 with its host reanalysis, ERA5, as well as the earlier hydrostatic 10-km Norwegian Hindcast Archive (NORA10; Reistad et al. 2011). The latter is included in the comparison mainly because it covers the same geographical domain and has been used extensively

(Aarnes et al. 2012; Furevik and Haakenstad 2012). Section 5 discusses the results and presents our conclusions.

## 2. Model setup

The NORA3 hindcast archive (Haakenstad et al. 2021; Solbrenkke et al. 2021) is generated with the nonhydrostatic C-P numerical weather prediction model HARMONIE-AROME, version 40h1.2 (Bengtsson et al. 2017), by solving the fully compressible Euler equations (Bénard et al. 2010). Modifications for high latitudes are included in the microphysics to reduce 2-m temperature bias and to improve low-level cloudiness (Müller et al. 2017b).

HARMONIE-AROME is forced with atmospheric fields from ERA5, having a horizontal resolution of approximately 31 km (Hersbach et al. 2020). Nine-hourly forecasts are calculated every sixth hour (initialized at 0000, 0600, 1200, and 1800 UTC), in which every cycle starts from a first guess, that is, the last forecast valid at the start of the new forecast. This first guess is corrected against observations in a surface assimilation scheme based on observations of 2-m temperature

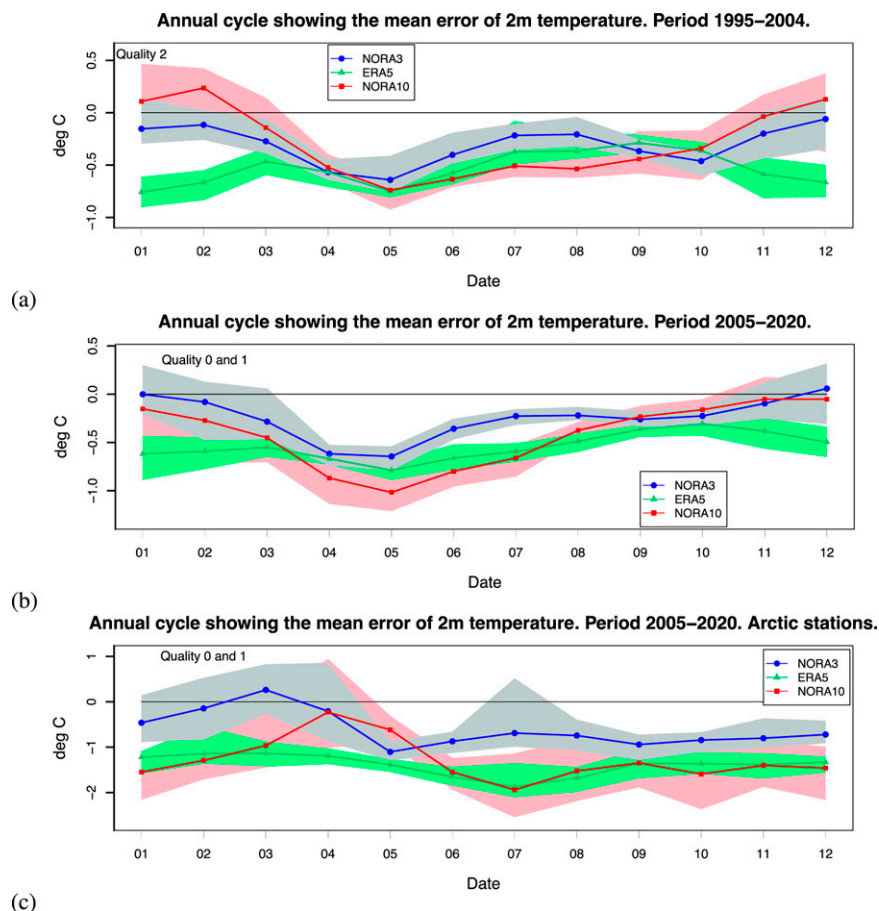


FIG. 3. Annual cycle of the monthly mean error in T2m (a),(b) for the mainland and (c) for Arctic stations for the period shown in (b). The annual cycle is shown with 90% confidence limits based on a nonparametric bootstrap procedure.

(T2m), 2-m relative humidity, and snow depth. The procedure is described by Le Moigne (2012), Müller et al. (2017b), and Haakenstad et al. (2021). (Because of reduced availability of snow observations, the snow field is only assimilated once daily.)

HARMONIE-AROME runs the surface model Surface Externalisée (SURFEX), see Masson et al. (2013). Snow is handled by a simple one-layer snow scheme called D95, described by Douville et al. (1995), and the sea ice is handled by a simple sea ice model (SICE; Batrak and Müller 2018). SICE requires a predefined sea ice concentration, which is here taken from ERA5 (Hersbach et al. 2020; Hirahara et al. 2016). The water surface temperatures of lakes are kept constant during the forecast. This is considered an acceptable simplification given the short length of the forecast runs. The interaction between soil, biosphere, and atmosphere is represented by the ISBA model (Boone et al. 1999), where the soil is characterized by three layers. (The vegetation is only described by one patch.) Subgrid runoff over saturated areas only happens when saturation is reached, using the variable infiltration capacity scheme, described in Habets et al. (1999).

NORA3 uses the Global Multiresolution Terrain Elevation Data (GMTED2010; see Danielson and Gesch 2011), with a

resolution of 7.5 arc s (about 250 m) for its orography. The GMTED2010 information is used to represent the mean elevation within a grid square of the model and also the shape of the orography (<http://www.umr-cnrm.fr/surfex/IMG/pdf/surfex-v7-3.pdf>). The orography can also affect radiation fluxes at surface levels (through shadowing and sky-view factors; see Senkova et al. 2007; Manners et al. 2012). However, these are not implemented in SURFEX, version 7.3, used here.

Upper-air temperature, specific humidity, and the zonal and meridional wind components required at the start of every forecast cycle are taken from ERA5. The remaining prognostic upper-air variables are taken from the previous forecast valid at the start of the new forecast.

A detailed documentation of the model setup is given by Haakenstad et al. (2021). An overview of the model setup for NORA3, together with the host model (ERA5) and the hydrostatic hindcast (NORA10), can be found in Table A1 in appendix A.

### 3. Observations

The station observations used in the validation of T2m and precipitation have been retrieved from the Frost

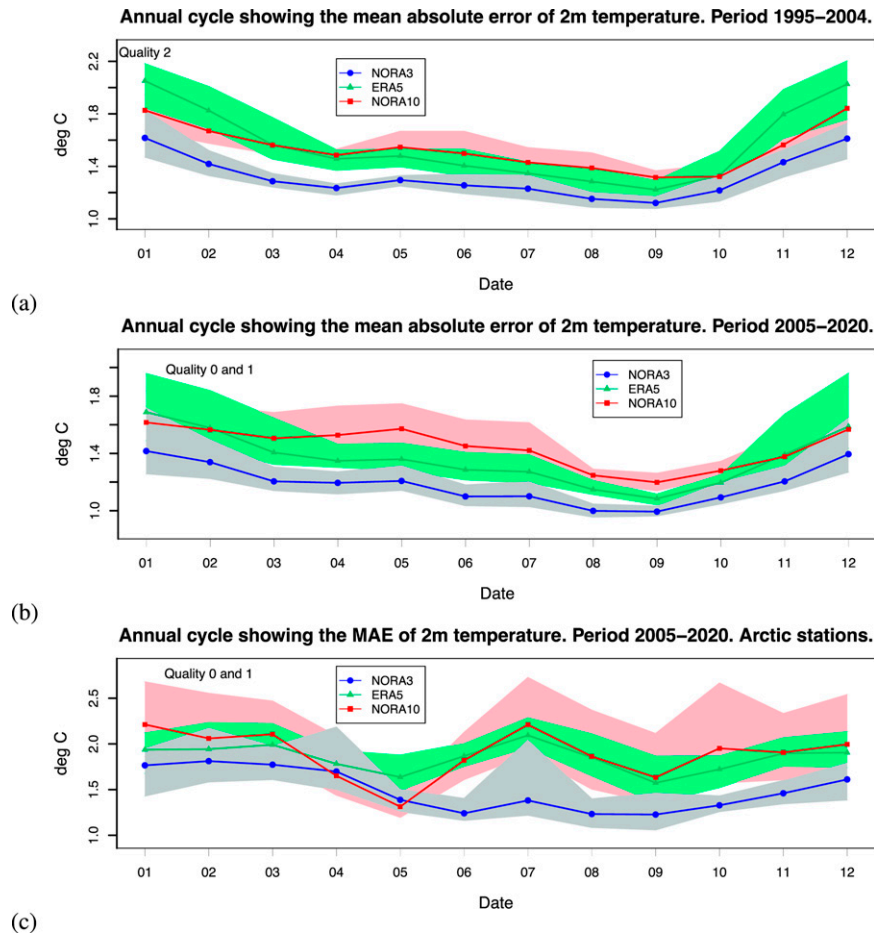


FIG. 4. As in Fig. 3, but for MAE.

database (<https://frost.met.no>), maintained by the Norwegian Meteorological Institute. The observations are quality controlled (Kjelland 2005).

#### a. Station observations of 2-m temperature

All stations measuring T2m that satisfy the following three criteria are used in the following comparison. The first requirement is based on a quality assessment. Since all observations of air temperature before 2005 are of unknown quality, the period 1995–2020 is divided into two, with unknown quality in the first period 1995–2004, while the two best quality categories are used in the period 2005–20. (The quality flags are documented at <https://frost.met.no/dataclarifications.html>.) The second requirement is for the stations to have nearly continuous time series, covering all the years in the period in question (years 1995–2004 for the observations of unknown quality and 2005–20 for the high-quality observations). The third requirement is that the height of the station should be in reasonable agreement with the corresponding height in NORA3, ERA5, and NORA10. The station is rejected if the height of the station differs by more than 200 m from the corresponding height of the nearest grid point in NORA3, ERA5, or NORA10. All stations shown in Fig. 1 fulfill these criteria.

#### b. Station observations of precipitation

A detailed description of the precipitation gauges in use in Norway is given by Køltzow et al. (2020). Unlike the temperature observations, all of the observations of precipitation in the period 1995–2020 are of known quality. The undercatch problem of solid precipitation (Rasmussen et al. 2012; Køltzow et al. 2019) is treated as outlined in appendix B. We corrected 7.6% of the observations for wind-snow conditions. Using the observations of best quality, only 0.026% of the observations have been rejected because of excessive deviations from any of the three datasets NORA3, ERA5, or NORA10 (the threshold was set to  $75 \text{ mm day}^{-1}$ ). We have also excluded months with fewer than 400 observations. This left out March 2004.

## 4. Results

### a. Temperature

NORA3 has been compared with in situ observations (see section 3) using a bilinear interpolation from the NORA3 model grid to the observation point (and similarly for ERA5 and NORA10). The nearest-neighbor method was also tested,

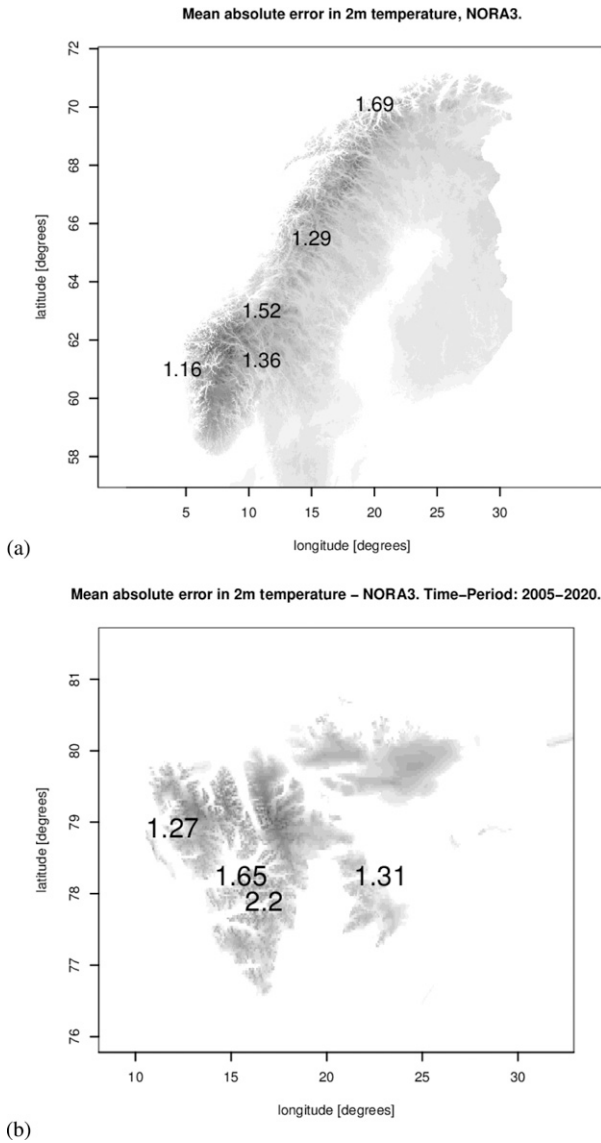


FIG. 5. (a) MAE in T2m for NORA3 for (a) the five regions on the Norwegian mainland and (b) the four stations on Svalbard [note the shorter time period in (b)].

but the bilinear interpolation method showed somewhat better performance for all the datasets, with a 0.6% improvement in the root-mean-square error (RMSE) of NORA3, a 5.7% improvement for ERA5 and 2.4% improvement in NORA10. Observations deviating by more than 20 K from either NORA3, ERA5, or NORA10 were rejected. These are normally erroneous observations and occur mainly in the first time period (1995–2004) where the observations have unknown quality since the quality flag is missing. (Rejected observations are listed in Table B1 in appendix B.)

Lead times from +4 to +9 h from the 6-hourly cycles of NORA3 and NORA10 were concatenated to form a continuous sequence, whereas hourly fields from the two analysis cycles (0600 and 1800 UTC) were selected from ERA5. Lead

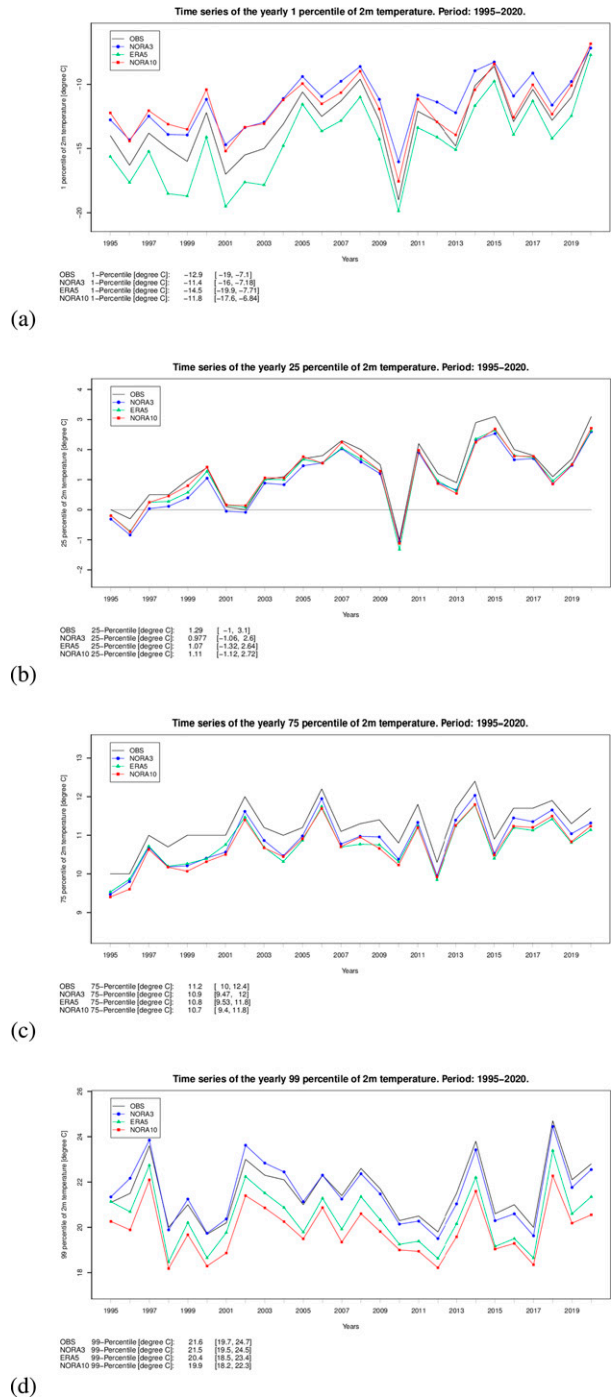


FIG. 6. ETS for T2m (°C) for mainland stations for four different percentiles. NORA3 is in blue, ERA5 is in green, and NORA10 is in red. Note that (a) presents negative values (below freezing) of T2m whereas (b) presents positive values of T2m. The period is 1995–2020.

times from +4 to +9 h in NORA3 and NORA10 were selected because they were found to systematically perform better than the earlier lead times. This is consistent with earlier studies of the performance of NORA10, see Reistad et al. (2009) for

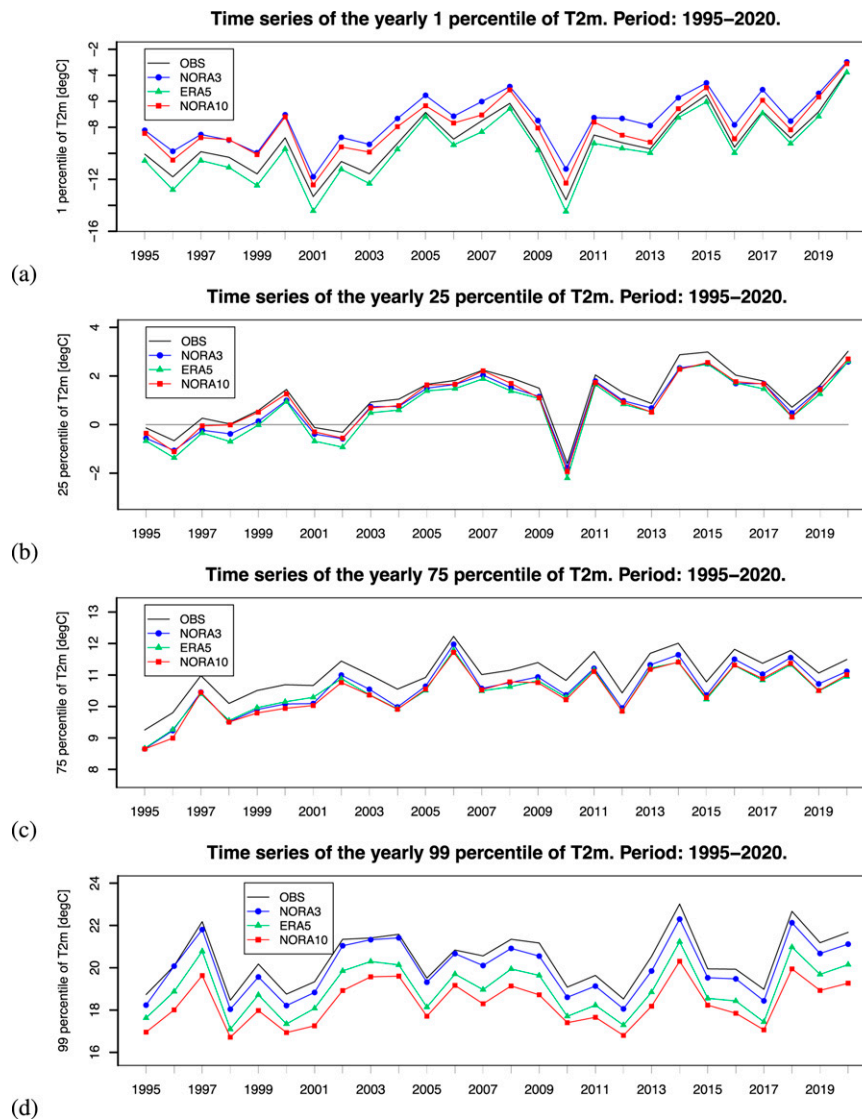


FIG. 7. Time series of the (a) 1st, (b) 25th, (c) 75th, and (d) 99th percentile of T2m ( $^{\circ}\text{C}$ ). Percentiles are calculated for each station before averaging.

wind speed performance showing a smaller mean error and a smaller root-mean-square error for the 6-h lead time, relative to the analysis and the 12-h lead time.

Figure 2a shows the scatter density plot of NORA3 versus observed T2m. The corresponding results for ERA5 and NORA10 are shown in Figs. 2b and 2c, respectively.

The correlation against T2m is found to be very high for all three datasets, with NORA3 slightly ahead at 0.972 and with an RMSE of 1.74 K. ERA5 shows a correlation of 0.962 to the observations and a slightly higher RMSE of 2.1 K. The correlation between NORA10 and observations is 0.960 with an RMSE of 2.1 K.

Figures 3 and 4 show the annual cycle of mean error and mean absolute error in T2m for the Norwegian mainland stations (Figs. 3a,b and 4a,b) and Arctic stations (Figs. 3c and 4c). The validation is divided into the two periods 1995–2004

(Figs. 3a and 4a) and 2005–20 (Figs. 3b and 4b) as explained in section 3, with the most reliable measurements in the later time period where observations are quality flagged. The 90% confidence intervals are shown as colored bands (gray-blue denotes NORA3, green denotes ERA5, and red denotes NORA10). The confidence intervals have been calculated with 100 iterations of a bootstrap procedure whereby the values of one random year are substituted by the values of another random year.

NORA3 outperforms ERA5 and NORA10 in all seasons but is still biased low (negatively). This result is found to be statistically significant with 90% confidence from spring to summer (see Fig. 4b) for the Norwegian mainland.

The strongest underestimation occurs in April and May. ERA5 shows a stronger year-round negative bias in T2m with the strongest negative bias in spring and weakest in autumn.

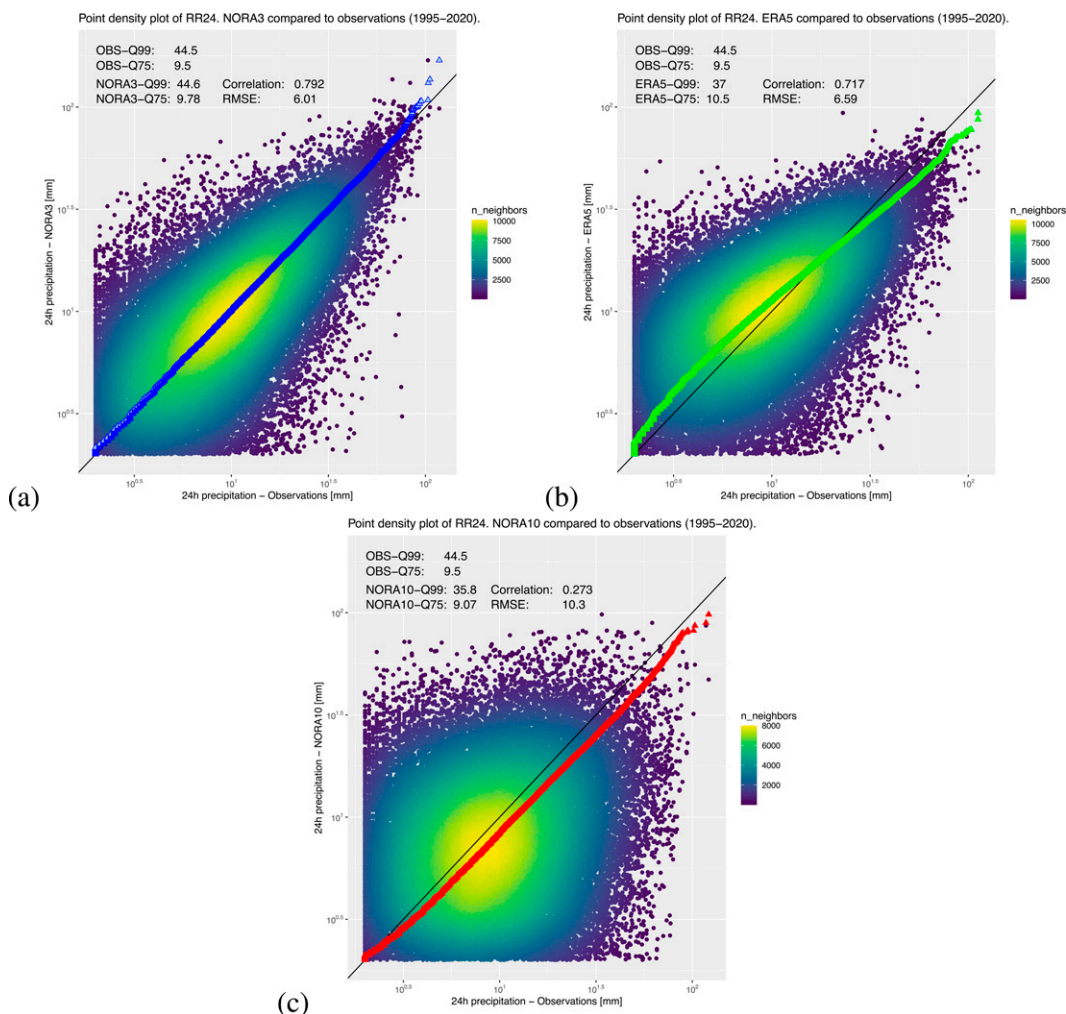


FIG. 8. Scatter density plot of 24-h precipitation for (a) NORA3, (b) ERA5, and (c) NORA10 in comparison with observations. Only observations exceeding  $2 \text{ mm (24 h)}^{-1}$  are shown (these constitute 436 868 observations). The statistics (i.e., quantiles 75 and 99 as well as correlation and RMSE) are based on all observations above the threshold limit of  $0.1 \text{ mm (24 h)}^{-1}$  (counting 1 057 422 observations; these are observations of the highest quality).

As for NORA3 and ERA5, NORA10 also shows the strongest underestimation in spring, but in wintertime, NORA10 overestimates the 2-m temperature. Upon inspection of Figs. 4a,b, we see that the mean absolute error (MAE) has been reduced by typically 0.2 from the first period to the second period. This is probably due to improved quality of the observations. For the Arctic, the results show higher uncertainty, with broader 90% confidence intervals, seen in both Figs. 3c and 4c.

Figure 5 shows the MAE averaged over five regions (see Fig. 1) of the Norwegian mainland for NORA3 (Fig. 5a). The regions are loosely based on the categorization by Hanssen-Bauer and Nordli (1998), with each region having fairly homogeneous long-term temperature variations. Only stations in the highest quality category have been used in the statistics (see turquoise dots in the map in Fig. 1).

Note that the two northernmost regions are merged and somewhat extended because of a scarcity of observations in

this area. The areas are, from north to south, 1) the northeastern coast and northern inner area counting 5 stations, 2) the northern coastal area with 23 stations, 3) the middle area counting 18 stations, 4) the southwestern coast counting 17 stations, and 5) the southeastern area with 34 stations. NORA3 performs best at the southwestern coast and shows the worst performance at the northeastern coast and northern inner area. A comparison with ERA5 and NORA10 is found in Fig. C1 in appendix C in which it is seen that ERA5 has an MAE that is 60% higher than that of NORA3.

Areas 1 and 2 in Fig. C1 (see appendix C) show statistically significant values within a 90% confidence interval, whereas mid- and southern Norway do not have statistically significant values within the 90% confidence interval. This has been calculated using a bootstrap procedure with 100 iterations, where in each iteration the value of a random station has been substituted by another random station value belonging to the specific area. Table C1 in appendix C shows the 90%



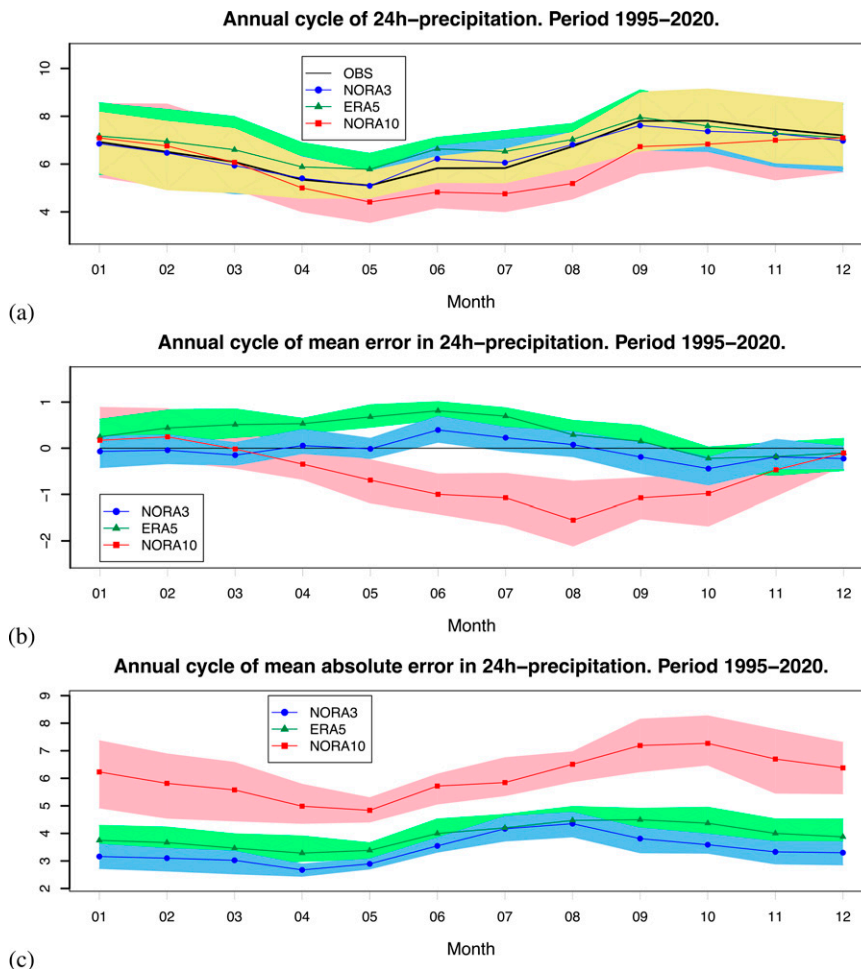


FIG. 9. (a) Annual cycle of daily precipitation, (b) its mean error, and (c) its MAE. Only days with precipitation have been taken into account in these annual cycles. The 90% confidence limits based on a nonparametric bootstrap procedure are overlaid.

confidence interval of MAE of T2m for NORA3, ERA5, and NORA10.

Figure 5b shows the MAE of NORA3 in the four stations in Svalbard. Because of the scarcity of observations, we have here plotted the individual stations rather than collecting them in regions and have not performed significance testing. However, the statistics are based on the number of observations listed in Table B2 in appendix B. Only quality-flagged stations are used here—hence only after 2004. NORA3 outperforms ERA5 in three of four stations. NORA3 outperforms NORA10 in all four stations (see Fig. C2 in appendix C).

Figure 6 presents the T2m equitable threat score (ETS) for NORA3, ERA5, and NORA10. The ETS is also known as the Gilbert skill score (Gandin and Murphy 1992; Wilks 2006). It is a categorical score; that is, it classifies a hit or miss, determined by a threshold value [see also the ETS of NORA3 10-m wind speed presented by Haakenstad et al. (2021)]. As we investigate exceedances above or below thresholds, it is necessary to divide the temperature dataset into two categories, negative (Fig. 6a) and positive (Fig. 6b) temperatures

(i.e., below or above 0°C). NORA3 performs very well for temperatures above −10°C, but is outperformed by ERA5 for temperatures below −15°C. This could be due to differences in the surface analysis schemes in ERA5 and NORA3 but could also in part be related to double-penalty effect in regions with steep topography. Table B3 in appendix B shows the number of observations for each T2m threshold value. The table shows that the ETS becomes significantly less robust in the high and the low end of the T2m threshold values because of the low number of observations.

Figure 7 shows the time series of the 1st (Fig. 7a), 25th (Fig. 7b), 75th (Fig. 7c), and 99th (Fig. 7d) percentile of T2m based on the observation from the stations given in Table B4 of appendix B.

The percentiles have been calculated for each station, and the values shown are yearly station-mean values of the percentiles. Both NORA3 and NORA10 overestimate the first percentile, whereas ERA5 shows a small underestimation. For the 25th percentile (Fig. 7b), there is a better agreement between the models, but with a weak underestimation. The

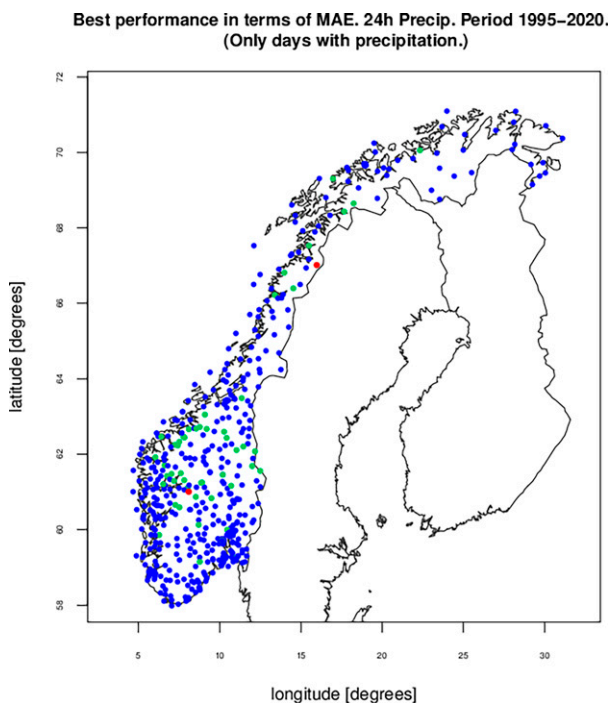


FIG. 10. Best performance in terms of MAE of 24-h precipitation using only days with precipitation. Blue, green, and red circles indicate best performance by NORA3, ERA5, and NORA10, respectively.

75th percentile (Fig. 7c) shows also a high agreement between the models, with a marginally better performance by NORA3. For the 99th percentile (Fig. 7d), NORA10 shows a marked underestimation. ERA5 is also clearly underestimating the 99th percentile, while NORA3 shows close agreement with the observations.

We have also compared the 2-m temperature in NORA3 with E-OBS (Cornes et al. 2018), the largest available gridded pan-European observational dataset (see appendix E). However, because of the coarser resolution of E-OBS ( $0.1^\circ$ ), it is difficult to make a direct comparison of NORA3 and E-OBS in complex terrain. It is, however, clear that NORA3 compares well in regions with gentler orography (especially Ireland, Denmark, England, and northwestern Germany; see the 99th percentile map in Fig. E2c in appendix E).

#### b. 24-h precipitation

The evaluation of daily (24 h) precipitation (RR24) is, similarly to the evaluation of T2m, based on a bilinear interpolation of NORA3, ERA50, and NORA10 to the observation points. Hourly precipitation is aggregated to 24-hourly quantities by using the lead times from +4 to +9 h for NORA3 and NORA10 from the four daily cycles (0000, 0600, 1200, and 1800 UTC). For ERA5, lead times from +7 to +18 have been used from the two cycles 0600 and 1800 UTC. We have chosen to focus on daily precipitation (RR24) because this averages the behavior at the different lead times from the three archives, NORA3, ERA5, and NORA10. Also, it reduces the

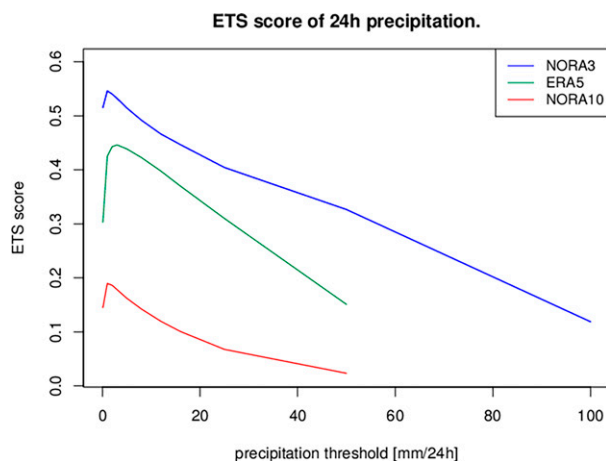


FIG. 11. ETS of 24-h precipitation.

impact of the double penalty on high-resolution model fields. A high-resolution model is likely to misplace a rainfall episode by a time step or may dislocate local rainfall slightly in space. This effect becomes worse with increasing resolution simply because a coarser model does not resolve the features in the same great detail. However, it does not mean that the coarser model in sum performs better. Thus, aggregated rainfall gives a fairer comparison of models with differing spatial resolution.

The scatter density plot of RR24 found in Fig. 8 shows that NORA3 and ERA5 are in very good agreement with the observations. NORA3 has a very good match to the 99th percentile ( $44.5 \text{ mm day}^{-1}$  observed and  $44.6 \text{ mm day}^{-1}$  for NORA3). The 75th percentile of NORA3 also fits the observations very well. NORA3 has the highest correlation and the lowest RMSE when compared with ERA5 and NORA10.

The annual cycle of the 24-h precipitation is shown for all three datasets and the observations in Fig. 9a. The observations show an average annual precipitation rate of  $6.6 \text{ mm day}^{-1}$ . (Only wet days are then counted, and we define a wet day as one with at least  $0.1 \text{ mm day}^{-1}$ .) We see, as expected, a marked annual cycle in daily precipitation. Days with precipitation show on average 17% more precipitation in autumn (SON) than the yearly average for days with precipitation. The value is 7% for winter (DJF). Least precipitation per wet day is found in spring (MAM), and summer (JJA) shows approximately 6% less precipitation per wet day when compared with the yearly average. On average there is almost 25% more precipitation in the autumn (SON) when compared with the yearly average, and 27% less in the spring (MAM).

NORA3 has almost no bias in the annual cycle of daily precipitation (Fig. 9b), though a weak positive bias can be seen in summer and a weak negative bias in autumn. ERA5 shows a positive mean error, except for the months October–December, when the bias is weakly negative. NORA10 shows a significant negative bias from April throughout October. NORA3 has lower mean absolute errors (Fig. 9c) than ERA5, and much lower than NORA10.

Figure 9 is based on the number of wet observations shown in Fig. B1 in appendix B. As can be seen in Fig. B1, there has

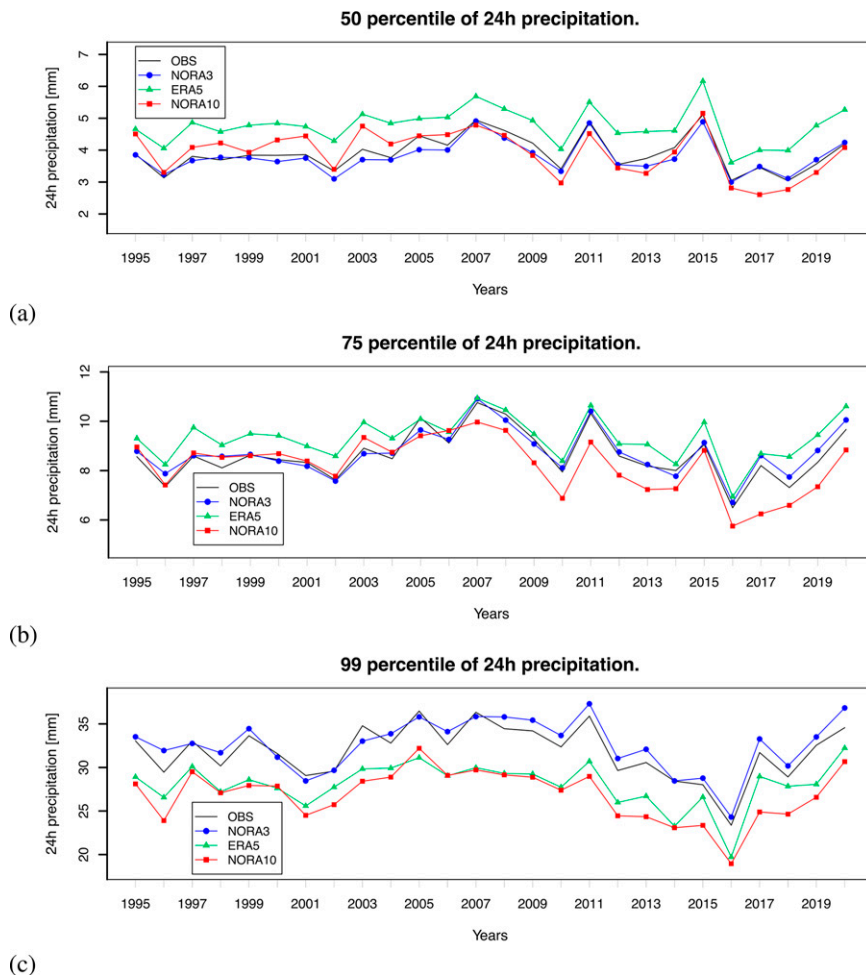


FIG. 12. Time series of the (a) 50th, (b) 75th, and (c) 99th percentile of 24-h precipitation interpolated to the Norwegian station network.

been a substantial increase in the number of observations in the last part of the period, 1995–2020. All datasets show slightly worse ME and MAE in the last decade of the period (not shown), connected to the increase in the observation network, as more high-precipitation events are captured.

Figure 10 summarizes the station-by-station performance in terms of MAE of RR24 when only wet days are considered. The map shows that NORA3 performs best in a majority of the stations. ERA5 shows the lowest MAE in 50 of, in total, 499 stations (and the number is even less when looking at all observations and also those lacking precipitation). The six Arctic stations (Bjørnøya, Hopen, Hornsund, Sveagrauva, Svalbard Airport, and Ny-Ålesund) are not shown in the map, since NORA3 shows the best performance in all the stations (for all measurements and also when only wet days are counted). The average MAE values for the Arctic stations are 0.9, 1.3, and 2.1 mm day<sup>-1</sup> for NORA3, ERA5, and NORA10, respectively, using all measurements. The values are naturally higher for wet days; 1.9, 2.4, and 3.0, respectively. The average MAE for the mainland stations is considerably higher; 1.9, 2.4, and 4.2, respectively, and

correspondingly 3.4, 3.9, and 6.0 for wet days. The higher MAE for the mainland stations is explained by the higher annual precipitation in mainland Norway. Figure 11 shows the ETS of different threshold values of 24-h precipitation. A performance that is significantly higher ranked is seen for NORA3 when compared with ERA5 and NORA10. NORA10 scores particularly poorly, which has been evident also in Figs. 8–10. All the datasets show highest scores for precipitation amounts less than 5 mm day<sup>-1</sup>, and the performance falls steeply with higher daily precipitation. (The number of observations falling within each threshold category is shown in Table B3 in appendix B.)

Figure 12 presents the time series of the 50th, 75th, and 99th percentile of RR24. NORA3 fits very well to the observations for all the percentiles shown. ERA5 shows a typical overestimation of the 50th and 75th percentiles, but an underestimation of the 99th percentile. This is also in agreement with Fig. 11c, showing that ERA5 has difficulties representing high precipitation (here exceeding 40 mm day<sup>-1</sup>). See also Müller et al. (2017b) in which ECMWF's IFS was found to

systematically misrepresent precipitation events exceeding  $15 \text{ mm} (12 \text{ h})^{-1}$ .

It is worth mentioning that NORA3 performs very well up to the 99th percentile and also up to the 99.5th percentile (not shown), but when exceeding the 99.9th percentile it tends to overshoot. This is shown in Fig. D1 in appendix D. The observed average 100th percentile for the 26 years is  $104 \text{ mm day}^{-1}$ , whereas NORA3 has an average 100th percentile of  $130 \text{ mm day}^{-1}$ . (The 100th percentile of ERA5 is  $76 \text{ mm day}^{-1}$ .) The very highest values of NORA3 are thus found to be excessively high; see, for example, 2009 for which the observed 100th percentile was  $122 \text{ mm day}^{-1}$  whereas NORA3 reported a 100th percentile of  $191 \text{ mm day}^{-1}$ .

## 5. Discussion and concluding remarks

The improved temperature performance found for NORA3 is mostly explained by the nonhydrostatic physics and its much higher resolution relative to ERA5. Other factors such as assimilation into a much finer grid (also indirectly a consequence of higher resolution) and the choice of physical parameterizations also play a role, but it is clear that the resolution and the nonhydrostatic physics are the most important factors. It is thus an expected benefit and one of the main reasons for generating high-resolution hindcasts from coarser host reanalyses.

Higher resolution gives a better representation of the surface, including coastline, orography, vegetation, ice cover, and urbanization. The details of the surface representation are also essential to the modeling of surface temperature, as the quality of albedo fields and the radiation and latent and sensible heat fluxes between the surface and the overlying air strongly affect the atmospheric boundary layer. The temperature performance of NORA3 is shown in Figs. 3 and 5 (see also Figs. C1 and C2 in appendix C for the performance of ERA5 and NORA10). The superior performance of NORA3 when compared with ERA5 is also in agreement with the findings by Müller et al. (2017a), where AROME-Arctic was found to outperform IFS in the AROME-Arctic domain. Müller et al. (2017a) found only smaller differences between the nonhydrostatic model and ECMWF over the Svalbard Archipelago, but significant improvement was found over northern Norway when comparing AROME-Arctic with the deterministic [high-resolution (HRES)] and ensemble (ENS) configurations of IFS as well as with the older reanalysis ERA-Interim (Dee et al. 2011).

Note that differences exist between AROME-Arctic and NORA3 as the former runs a full analysis with a three-dimensional variational assimilation, whereas NORA3 runs a newer model cycle but only a surface analysis. Even so, the two models are dynamically very similar. Müller et al. (2017a) showed that AROME-Arctic has a better representation of the boundary layer under stable atmospheric conditions, whereas the ECMWF model configurations exhibited too deep boundary layers due to a too diffusive turbulence closure model.

Although the results show improved performance of T2m in NORA3 relative to ERA5 and NORA10, NORA3 still has

issues with springtime temperatures, which tend to be significantly underestimated. One reason is excessive evaporation in the HARMONIE-AROME model during springtime. This creates too-high relative humidity, which again results in too-low surface temperatures during daytime, as reported by Samuelsson et al. (2018). Improved T2m performance was found by introducing two patches over land, separating forest and open land. Samuelsson et al. (2018) also introduced a modified tree height dataset and increased the snow roughness length. Although these modifications were advantageous to the near-surface temperature, the first version of the upgrade also led to a deterioration of the wind speed, and the modifications were not included in the NORA3 configuration. Another reason for the underestimation of the 2-m temperature in spring could be too-long-lasting snow cover in areas where there are few observations and where the snow assimilation consequently has less influence. A third reason could also be related to the orographic influence on the radiative fluxes. The SURFEX version used for NORA3 does not include orographic effects on the radiation fluxes, such as the sky view factor and shadowing effects (Senkova et al. 2007), which also affect T2m significantly. Manners et al. (2012) found a 2.5 K temperature difference due to short wave effects under clear-sky conditions, and 1 K due to long-wave effects when analyzing the orographic effects on radiation fluxes. The orographic influence on radiation should primarily reduce the 2-m temperature, but it could also reduce the cooling in the valleys.

The superior performance in daily precipitation in NORA3 in compared with ERA5, and even more so when compared with NORA10, is also an expected benefit of the higher resolution of NORA3 and the use of a convection-permitting model. The improvement is, however, remarkable, particularly for the upper percentiles (see Figs. 11 and 12). It has been reported elsewhere (Diamantakis and Magnusson 2016) that ERA5 may be overstretching the time step for efficiency. This can have adverse effects on the precipitation performance, but it seems obvious that the improvement comes mainly from higher resolution and the use of a convection-permitting nonhydrostatic model.

This study concludes that a spatial resolution of 3 km is sufficient to resolve well the upper percentiles of precipitation in complex terrain. NORA3 does not incorporate a full reanalysis, and a future comparison with the forthcoming Arctic Regional Reanalysis (CARRA; see Yang et al. 2020; Køltzow et al. 2022), commissioned by the Copernicus Climate Change Service (C3S), will help to shed light on the importance of including assimilation of upper-air observations in modeling wind, temperature, and precipitation extremes.

Norway and the Svalbard Archipelago represent interesting test cases for nonhydrostatic C-P models with highly developed microphysics, both in terms of temperature and rainfall as their complex terrain experiences a large number of violent extratropical systems each year. This makes the interplay between the wind field and the terrain as well as the ice edge important. The NORA3 hindcast has been found in part I of this study to model the wind field and its probability distribution in complex terrain much better than its host analysis ERA5 (Haakenstad et al. 2021). Here we have shown that its performance in terms of surface temperature and in particular its precipitation is also

TABLE A1. Basic properties of NORA3, ERA5, and NORA10.

Name	NORA3	ERA5	NORA10
Type	Hybrid hindcast reanalysis; deterministic (D) (Haakenstad et al. 2021)	Reanalysis; D + lower-resolution ensembles (Hersbach et al. 2020)	Hindcast; D (Reistad et al. 2011)
NWP model	HARMONIE-AROME Cy40h1.2 (Seity et al. 2011; Brousseau et al. 2016; Bengtsson et al. 2017)	IFS Cy41r2; IFS documentation—Cy41r2 ( <a href="https://www.ecmwf.int/en/publications/search">https://www.ecmwf.int/en/publications/search</a> ; search term “cy41r2”)	HIRLAM, v.6.4.2 (Unden et al. 2002)
Domain	Limited area model (LAM) (northeast Atlantic)	Global	LAM (northeast Atlantic)
Grid	Spectral	Spectral	Grid point
Horizontal grid spacing	3 km	31 km (TL639)	10–11 km
No. of vertical levels	65 ( $\approx 12$ m–10 hPa)	137 [ $\approx 10$ m–1 Pa ( $\approx 80$ km)]	40 ( $\approx 27$ m–10 hPa)
Vertical coordinate	Hybrid sigma pressure ( $\sigma$ , $p$ )	$\sigma$ , $p$	$\sigma$ , $p$
Dynamical core	Nonhydrostatic (Bubnová et al. 1995; Bénard et al. 2010)	Hydrostatic	Hydrostatic
Advection scheme	Semi-Lagrangian (SL)	SL	SL
Vertical discretization	Finite element	Finite difference	Finite difference
Time step	60 s	720 s	240 s
Cycle frequency	6 hourly	12 hourly	6 hourly
Forecast range	9 h	18 h	9 h
Analyses	6 hourly	Hourly	6 hourly
Surface assimilation	Code d'Analyse Nécessaire à ARPEGE pour ses Rejets et son Initialization (CANARI) (Le Moigne 2012)	Advanced land DA system (de Rosnay et al. 2014)	No
Background Observations	Optimum interpolation-main (Daley 1991) Land and sea surface retrieved from the ECMWF Meteorological Archival and Retrieval system (MARS)	See Hersbach et al. (2020)	Latest forecast None
Atmospheric data assimilation	None	4D-VAR 12-h window	None
Host model	ERA5	None	ERA40 + IFS-Ana
Coupling method	Simple interpolation to grid		Blending (Yang 2005)
Physiography	ECOCLIMAP, v.2 (Faroux et al. 2013)	Different datasets; IFS documentation—Cy41r2 Part IV: Chapter 11 ( <a href="https://www.ecmwf.int/en/elibrary/16648-ifs-documentation-cy41r2-part-iv-physical-processes">https://www.ecmwf.int/en/elibrary/16648-ifs-documentation-cy41r2-part-iv-physical-processes</a> )	Different datasets; details in Unden et al. (2002)
Orography	GMTED2010; 250 m	Mixed GLOBE with other datasets; 1 km	GTOPO30; 1 km
Microphysics	ICE3 (Pinty and Jabouille 1998; Lascaux et al. 2006); O-Condensation-2 (OCND2) (Müller et al. 2017a); Kogan autoconversion (Khairoutdinov and Kogan 2000)	Cy36r4-onward-scheme (Forbes et al. 2011)	Extended Sundqvist scheme (Sundqvist 1993)
Turbulence	HARMONIE with RACMO Turbulence (HARATU) (van Meijgaard et al. 2012; Lenderink and Holtslag 2004)	IFS documentation—Cy41r2 Part IV: Chapter 3 ( <a href="https://www.ecmwf.int/en/elibrary/16648-ifs-documentation-cy41r2-part-iv-physical-processes">https://www.ecmwf.int/en/elibrary/16648-ifs-documentation-cy41r2-part-iv-physical-processes</a> )	TKE-I (Cuxart et al. 2000)
Radiation	Longwave, RRTM (Mlawer et al. 1997); ECMWF shortwave scheme (ECMWF 1989)	RRTM (Mlawer et al. 1997; Iacono et al. 2008)	Fast radiation parameterization (Savijärvi 1990)
Convection	Eddy-diffusivity mass-flux (EDMF)-M (Siebesma et al. 2003, 2007; Soares et al. 2004; de Rooy and Siebesma 2010)	IFS documentation—Cy41r2 Part IV: Chapter 6.4 (Bechtold et al. 2014)	Soft Transition Condensation (STRACO) (Kuo 1974)
Surface modeling	SURFEX (Masson et al. 2013)	HTESSEL (Balsamo et al. (2009)	Mosaic of tiles (Avissar and Pielke 1989; Bringfelt et al. 1999)

TABLE B1. Number of temperature observations rejected (R) each year because of a difference between observations and NORA3, ERA5, or NORA10 of more than 20 K, and the total number of rejected observations in the whole time period and in the two periods 1995–2004 and 2005–20 (last three rows).

Year	No. of stations	Total No. of obs	R by NORA3	R by ERA5	R by NORA10	R totally
1995	104	811 254	494	808	558	820
1996	104	1 128 890	106	178	116	192
1997	104	1 288 978	42	46	42	52
1998	104	1 294 880	68	82	70	86
1999	104	1 322 054	88	102	80	102
2000	104	1 357 310	76	78	70	84
2001	104	1 555 250	56	82	118	150
2002	104	1 550 600	38	44	36	50
2003	104	1 789 126	104	122	92	142
2004	104	1 963 664	186	178	182	198
2005	92	1 348 343	0	0	0	0
2006	92	1 488 830	1	3	1	3
2007	92	1 504 582	0	0	74	74
2008	92	1 569 945	1	1	1	1
2009	92	1 583 168	0	0	0	0
2010	92	1 566 966	126	28	136	286
2011	92	1 587 456	0	0	0	0
2012	92	1 598 171	0	0	0	0
2013	92	1 584 558	0	0	18	18
2014	92	1 591 519	0	8	0	8
2015	92	1 584 743	0	0	0	0
2016	92	1 586 896	10	6	0	10
2017	92	1 564 820	0	0	0	0
2018	92	1 562 812	0	0	0	0
2019	92	1 563 514	0	0	0	0
2020	92	1 582 382	0	0	0	0
1995–2020		38 930 711	1582	1134	534	2276
1995–2004	104	14 062 006	1294	760	190	1876
2005–2020	92	24 868 705	288	374	344	400

markedly improved relative to its host reanalysis. This makes the hindcast well suited for studies of terrestrial extreme events where steep topography and complex coastlines affect the passage of extratropical cyclones, but also for studies of the mesoscale conditions associated with extreme rainfall and temperature extremes.

*Acknowledgments.* This study was carried out with support from the ERA4CS WINDSURFER project and the Norwegian Climate Service Centre (KSS). We gratefully acknowledge the support from Equinor ASA who cofunded the development of the NORA3 archive. We also acknowledge support from the Research Council of Norway through the Stormrisk project (Grant 300608). We are grateful for funding from the Norwegian Public Roads Administration through the project “Ferjefri E-39.” We acknowledge the E-OBS dataset from the EU-FP6 project UERRA (<http://www.uerra.eu>) and the Copernicus Climate Change Service, and the data providers in the ECA and R project (<https://www.ecad.eu>).

*Data availability statement.* The data are archived in NetCDF on the Norwegian Meteorological Institute’s publicly accessible Thredds server (<https://thredds.met.no/thredds/projects/nora3.html>). Quality-assured observing stations used in this study are retrieved from the Norwegian Meteorological Institute’s observation database (<https://frost.met.no>).

## APPENDIX A

### Technical Specifications of NORA3, ERA5, and NORA10

A summary of technical specifications of the hindcasts and the reanalysis used in the study is given in [Table A1](#).

## APPENDIX B

### Details about the Observations

The annual tally of 2-m temperature measurements as well as the number of rejected measurements is listed in [Table B1](#). [Figure B1](#) lists the number of dry and wet observations by month. The undercatch of solid precipitation is treated using the following correction factor [Eq. (13) by [Wolff et al. \(2015\)](#)]:

$$c = \left[ 0.82 - \frac{0.81e^{(T-0.66)/1.07}}{1 + e^{(T-0.66)/1.07}} \right] e^{(-V/4.24)^{1.81}} + \frac{0.81e^{(T-0.66)/1.07}}{1 + e^{(T-0.69)/1.07}} + 0.18. \quad (\text{B1})$$

All RR24 measurements that coincide with a daytime minimum temperature 2°C and a maximum wind speed exceeding 7 m s<sup>-1</sup>, (where the minimum temperature and the maximum

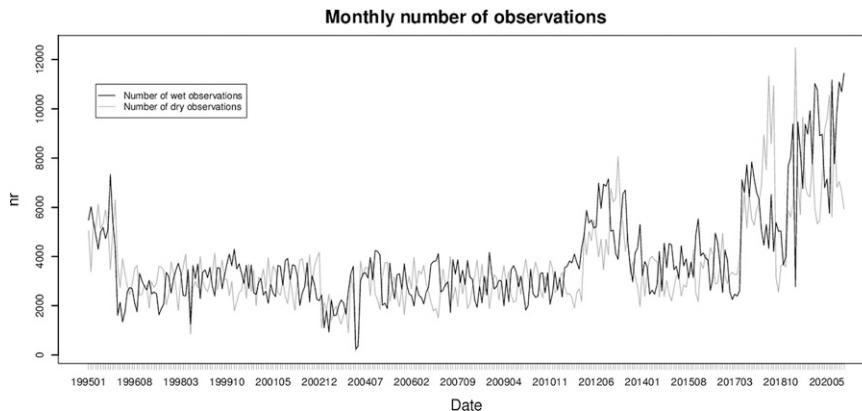


FIG. B1. The number of precipitation measurements used in the statistics.

wind speed are based on hourly values from NORA3), are corrected by using the daily mean wind speed and 2-m temperature from NORA3 in Eq. (B1). The mean wind speed has been reduced from 10 m to gauge height with a correction factor that is based on the logarithmic wind profile, assuming a gauge height of 2 m and a roughness length of 0.0002 m. Topographical features introduce an uncertainty in the representativeness of the wind speed related to the precipitation measurement, and therefore an upper limit on the correction factor has been set to 1.6 for temperatures below  $-2^{\circ}\text{C}$  and 1.4 for temperatures between  $-2^{\circ}$  and  $2^{\circ}\text{C}$  (Førland and Hanssen-Bauer 2000; Førland et al. 2020). Precipitation below  $1.0\text{ mm day}^{-1}$  is not corrected. All stations have been checked for wind-snow correction, except Haukelisetter, which has its instrument inside a double fence and is thus considered to require no correction. Two percent of the observations require a correction factor in the range 1.0–1.4, whereas 5.6% of the observations require a correction factor in the range 1.0–1.6.

Tables B2 and B3 provide the number of observations used for calculation of the MAE and ETS values of T2m, respectively. Lists of mainland stations that observe T2m are given in Table B4. Table B5 gives the number and distributions of observations used for calculation of the daily precipitation ETS.

APPENDIX C

Additional Results on T2m Performance

Figure C1 shows the relative difference (percent) between the T2m MAE of ERA5 and NORA3 (Fig. C1a)

TABLE B2. Number of observations used for calculation of the MAE values of T2m shown in Figs. 5b and C2 (below).

Station name	No. of obs
Edgeøya-Kapp Heuglin	92 880
Sveagruva	129 413
Svalbard Airport	134 105
Ny-Ålesund	133 186

and NORA10 and NORA3 (Fig. C1b). ERA5 has a relative MAE up to 61.7% higher than NORA3, and only in the southeastern area does ERA5 have an MAE comparable to NORA3. NORA10 has a relative MAE that is 14%–35% higher than NORA3. Figure C2 shows the MAE of ERA5 (Fig. C2a) and NORA10 (Fig. C2b) in Svalbard. Table C1 gives the 90% probability range of T2m MAE (K) for NORA3, ERA5, and NORA10 for the five different regions.

APPENDIX D

Additional Results of the Daily Precipitation Performance

The very highest RR24 percentiles, 99.5th, 99.9th, and 100th, are shown in Fig. D1. NORA3 clearly outperforms ERA5 and NORA10 also, except for the 100th percentile where NORA3 overestimates the RR24H.

TABLE B3. Number of observations used for calculation of the ETS of T2m shown in Fig. 6.

Category	No. of observations
Positive values of observed T2m	
Above $0^{\circ}\text{C}$	31 748 106
Above $5^{\circ}\text{C}$	21 315 321
Above $10^{\circ}\text{C}$	11 447 703
Above $15^{\circ}\text{C}$	3 786 003
Above $20^{\circ}\text{C}$	757 939
Above $25^{\circ}\text{C}$	748 964
Above $30^{\circ}\text{C}$	3844
Negative values of observed T2m	
Below $0^{\circ}\text{C}$	7 955 227
Below $-5^{\circ}\text{C}$	2 563 829
Below $-10^{\circ}\text{C}$	679 626
Below $-15^{\circ}\text{C}$	142 686
Below $-20^{\circ}\text{C}$	22 092
Below $-25^{\circ}\text{C}$	24 778
Below $-30^{\circ}\text{C}$	3219
Below $-35^{\circ}\text{C}$	556

TABLE B4. Mainland stations observing T2m (LH denotes lighthouse, and A denotes airport).

Station code	Name	Lon (°E)	Lat (°N)	County	Height (m)
SN11500:0	Østre Toten-Apelsvoll	10.87	60.70	Innlandet	264
SN12320:0	Hamar-Stavsberg	11.07	60.82	Innlandet	221
SN17000:0	Strømtange LH	10.83	59.15	Viken	10
SN17150:0	Rygge	10.80	59.37	Viken	40
SN18700:0	Oslo-Blindern	10.72	59.94	Oslo	94
SN20301:0	Hønefoss-Høyby	10.25	60.17	Viken	140
SN25830:0	Finsevatn	7.53	60.60	Vestland	1210
SN26900:0	Drammen-Berskog	10.12	59.75	Viken	8
SN26990:0	Sande-Galleberg	10.22	59.62	Vestfold og Telemark	60
SN27450:0	Melsom	10.35	59.23	Vestfold og Telemark	26
SN27500:0	Færder LH	10.52	59.03	Vestfold og Telemark	6
SN29720:0	Dagali A	8.53	60.42	Viken	798
SN30650:0	Notodden A	9.21	59.57	Vestfold og Telemark	20
SN32060:0	Gvarv-Nes	9.21	59.38	Vestfold og Telemark	93
SN34130:0	Jomfruland	9.57	58.86	Vestfold og Telemark	3
SN35860:0	Lyngør LH	9.15	58.64	Agder	4
SN36200:0	Torungen LH	8.79	58.40	Agder	12
SN38140:0	Landvik	8.52	58.34	Agder	6
SN39040:0	Kjevik	8.08	58.2	Agder	12
SN39100:0	Oksøy LH	8.05	58.07	Agder	9
SN40880:0	Hovden-Lundane	7.39	59.58	Agder	841
SN41770:0	Lindesnes LH	7.05	57.98	Agder	16
SN42160:0	Lista LH	6.57	58.11	Agder	14
SN43010:0	Eik-Hove	6.50	58.51	Rogaland	65
SN44080:0	Obrestad LH	5.56	58.66	Rogaland	24
SN44300:0	Særheim	5.65	58.76	Rogaland	87
SN44560:0	Sola	5.64	58.88	Rogaland	7
SN44610:0	Kvitsøy-Nordbø	5.41	59.07	Rogaland	21
SN47260:0	Haugesund A	5.21	59.34	Rogaland	24
SN47300:0	Utsira LH	4.87	59.30	Rogaland	55
SN48120:0	Stord A	5.34	59.79	Vestland	49
SN48330:0	Slåtterøy LH	5.07	59.91	Vestland	25
SN50070:0	Kvamsøy	6.28	60.36	Vestland	49
SN50500:0	Flesland	5.23	60.29	Vestland	48
SN50540:0	Bergen-Florida	5.33	60.38	Vestland	12
SN51530:0	Vossevangen	6.43	60.63	Vestland	54
SN52535:0	Fedje	4.72	60.75	Vestland	19
SN53101:0	Vangsnes	6.65	61.17	Vestland	49
SN55290:0	Sognefjellyhytta	8.00	61.57	Innlandet	1413
SN55820:0	Fjærland-Bremuseet	6.76	61.42	Vestland	3
SN56420:0	Fureneset	5.04	61.29	Vestland	7
SN57000:0	Førde	5.76	61.39	Vestland	321
SN57710:0	Florø A	5.03	61.58	Vestland	9
SN57770:0	Ytterøyane LH	4.68	61.57	Vestland	26
SN58100:0	Sandane A	6.10	61.83	Vestland	60
SN59110:0	Kråkenes	4.99	62.03	Vestland	75
SN59680:0	Ørsta-Volda A	6.08	62.18	Møre og Romsdal	74
SN59800:0	Svinøy LH	5.27	62.33	Møre og Romsdal	38
SN6020:0	Flisa II	12.01	60.61	Innlandet	185
SN60990:0	Vigra	6.12	62.56	Møre og Romsdal	22
SN62270:0	Molde A	7.26	62.74	Møre og Romsdal	3
SN62480:0	Ona II	6.54	62.86	Møre og Romsdal	20
SN63420:0	Sunnalsøra III	8.55	62.68	Møre og Romsdal	6
SN64330:0	Kristiansund A	7.82	63.11	Møre og Romsdal	62
SN65310:0	Veiholmen	7.95	63.52	Møre og Romsdal	5
SN65940:0	Sula	8.47	63.85	Trøndelag	5
SN68860:0	Trondheim-Voll	10.45	63.41	Trøndelag	127
SN69100:0	Værnes	10.93	63.46	Trøndelag	12
SN69150:0	Kvithamar	10.88	63.49	Trøndelag	27



TABLE B4. (Continued)

Station code	Name	Lon (°E)	Lat (°N)	County	Height (m)
SN700:0	Drevsjø	12.05	61.89	Innlandet	672
SN71000:0	Steinkjer-Søndre Egge	11.45	64.02	Trøndelag	6
SN71850:0	Halten LH	9.41	64.17	Trøndelag	16
SN71990:0	Buholmråsa LH	10.46	64.40	Trøndelag	18
SN72580:0	Namsos A	11.57	64.47	Trøndelag	2
SN75220:0	Rørvik A	11.14	64.84	Trøndelag	4
SN75410:0	Nordøyen LH	10.55	64.80	Trøndelag	33
SN75550:0	Sklinna LH	11.00	65.20	Trøndelag	23
SN76330:0	Brønnøysund A	12.22	65.46	Nordland	9
SN76530:0	Tjøtta	12.43	65.83	Nordland	21
SN76750:0	Sandnessjøen	12.48	65.96	Nordland	17
SN77230:0	Mosjøen A	13.22	65.78	Nordland	72
SN79600:0	Mo I Rana A	14.30	66.36	Nordland	70
SN80610:0	Myken	12.49	66.76	Nordland	17
SN82290:0	Bodø VI	14.36	67.27	Nordland	11
SN82410:0	Helligvær II	13.90	67.40	Nordland	24
SN84970:0	Evenes A	16.68	68.49	Nordland	26
SN85380:0	Skrova LH	14.65	68.15	Nordland	14
SN85450:0	Svolvær A	14.67	68.25	Nordland	9
SN85560:0	Leknes A	13.62	68.16	Nordland	26
SN85840:0	Værøy	12.72	67.65	Nordland	4
SN85890:0	Røst A	12.10	67.53	Nordland	4
SN86600:0	Stokmarknes	15.03	68.58	Nordland	3
SN86740:0	Bø I Vesterålen III	14.44	68.61	Nordland	8
SN87640:0	Harstad Stadion	16.54	68.80	Troms og Finnmark	45
SN88690:0	Hekkingen LH	17.83	69.60	Troms og Finnmark	33
SN90400:0	Tromsø-Holt	18.91	69.65	Troms og Finnmark	20
SN90450:0	Tromsø	18.94	69.65	Troms og Finnmark	100
SN90490:0	Tromsø-Langnes	18.91	69.68	Troms og Finnmark	8
SN93140:0	Alta A	23.36	69.98	Troms og Finnmark	3
SN94280:0	Hammerfest A	23.68	70.69	Troms og Finnmark	81
SN98550:0	Vardø Radio	31.10	70.37	Troms og Finnmark	10
SN98790:0	Vadsø A	29.84	70.07	Troms og Finnmark	39

## APPENDIX E

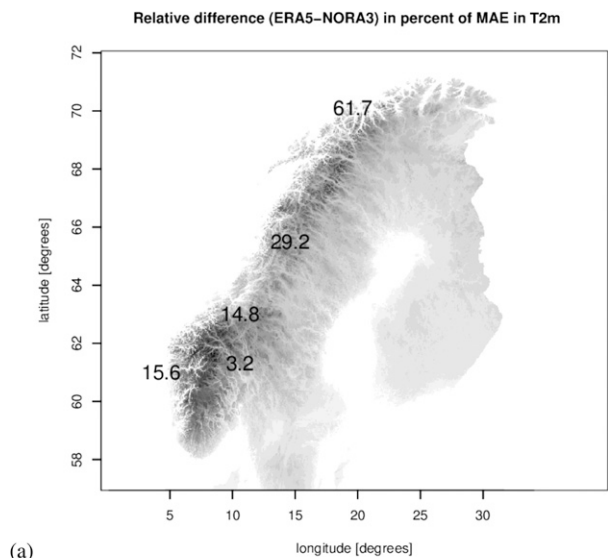
## E-OBS

E-OBS is the largest available gridded pan-European observational dataset. It consists of station measurements interpolated to a 0.1° regular grid (Cornes et al. 2018). Note

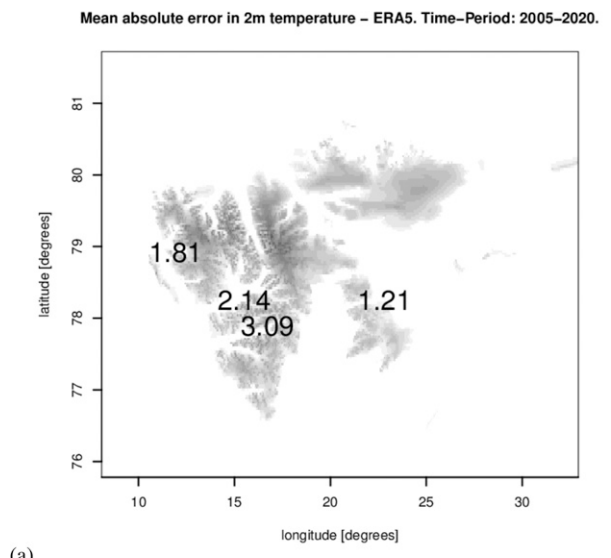
TABLE B5. Number of observations used for calculation of the daily precipitation ETS shown in Fig. 11.

Category	No. of obs
Above 0.1 mm	1339962
Above 1 mm	966581
Above 2 mm	792129
Above 3 mm	671187
Above 5 mm	502273
Above 8 mm	340845
Above 12 mm	213972
Above 16 mm	139060
Above 25 mm	57417
Above 50 mm	7061
Above 100 mm	164

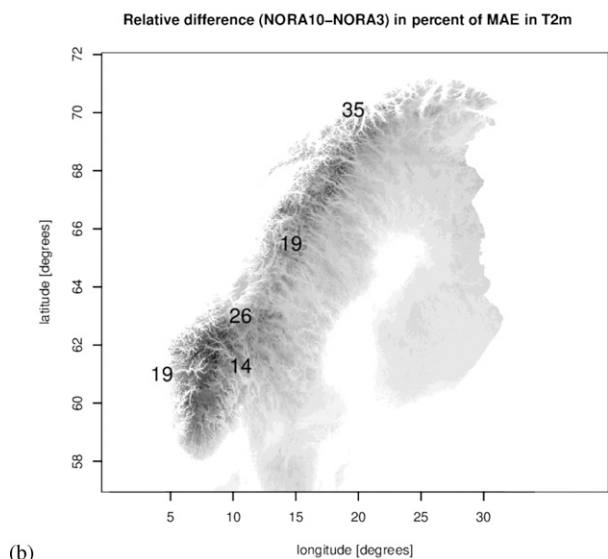
that E-OBS does not cover Svalbard. We have fetched v23.1e of the daily mean temperature and daily precipitation from the Copernicus Climate Change Service. Being a gridded product based on in situ measurements, its quality depends on the density. E-OBS is interpolated to a grid that is about 3 times as coarse as NORA3 and is not able to resolve fine-scale orographic details in steep terrain. It includes only grid cells that are entirely land covered, thus excluding the coastal zone. Also, the E-OBS dataset is not based on a homogeneous set of observing stations and the comparison with NORA3, ERA5, and NORA10 must therefore be interpreted with some caution. Figure E1 shows the E-OBS map of the first percentile of daily averaged 2-m temperature, 1P-T2m (Fig. E1a, and NORA3 is in Fig. E1b). The difference between NORA3 and E-OBS is presented in Fig. E1c, whereas the difference between ERA5 and E-OBS and NORA10 and E-OBS is shown in Figs. E1d and E1e, respectively. (The percentiles are based on the period 1995–2020.) The 1P-T2m has a strong west–east and south–north gradient with the lowest temperatures in the inner part of Finnmark, the northernmost county in mainland Norway. Along the west



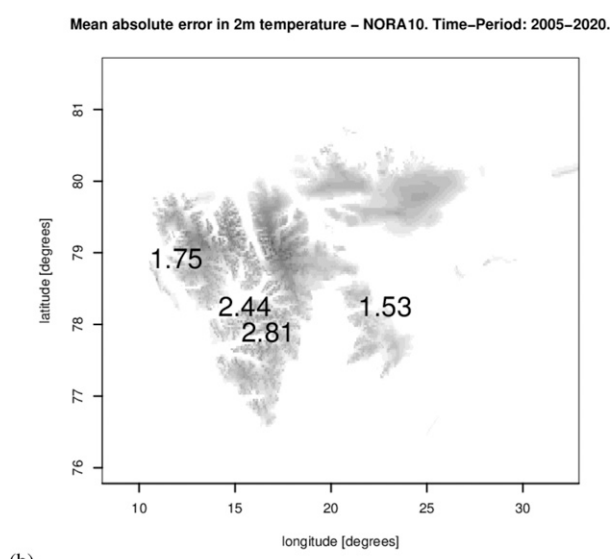
(a)



(a)



(b)



(b)

FIG. C1. Difference between MAE in 2Tm between (a) ERA5 or (b) NORA10 and NORA3 (percent) in the five regions of the Norwegian mainland.

coast of Norway the first percentile is typically  $-6^{\circ}\text{C}$ , while the inner part of southeastern Norway reaches  $-24^{\circ}\text{C}$ , and the inner part of Finnmark dips below  $-30^{\circ}\text{C}$ . NORA3 appears to be able to model very realistically the 1st-percentile

TABLE C1. The 90% probability range of MAE (K) for the five different regions: northeastern area (area 1), northern coastal area (area 2), middle area (area 3), southwestern coast (area 4), and southeastern area (area 5). The values are based on a bootstrapping procedure for the period 1995–2020.

	NORA3	ERA5	NORA10
Area 1	1.51–1.84	2.34–3.59	2.05–2.61
Area 2	0.99–1.68	1.29–2.19	1.28–1.95
Area 3	1.15–2.94	1.25–3.93	1.44–4.12
Area 4	0.91–1.73	1.04–2.06	1.11–2.27
Area 5	1.08–1.68	1.11–2.37	1.27–2.37

FIG. C2. MAE in T2m of (a) ERA5 and (b) NORA10 at the four stations in Svalbard.

T2m along the coast and in the southern part of Norway and generally in the lowlands, where the 1st percentile is above  $-18^{\circ}\text{C}$ , but the situation is different for the coldest regions. The overestimation becomes significant in the coldest areas inland and also in some mountainous regions and does not reach below  $-28^{\circ}\text{C}$  in Finnmark (the northernmost county of Norway). The overestimation of low temperatures inland is a well-known problem. Køltzow et al. (2019) showed that both AROME and the HRES operational forecast model of IFS with 9-km horizontal resolution performed poorly in calm, cold conditions, a frequent situation inland in Scandinavia during wintertime. Atlaskin and Vihma (2012) found that the models investigated (IFS, HIRLAM, AROME,

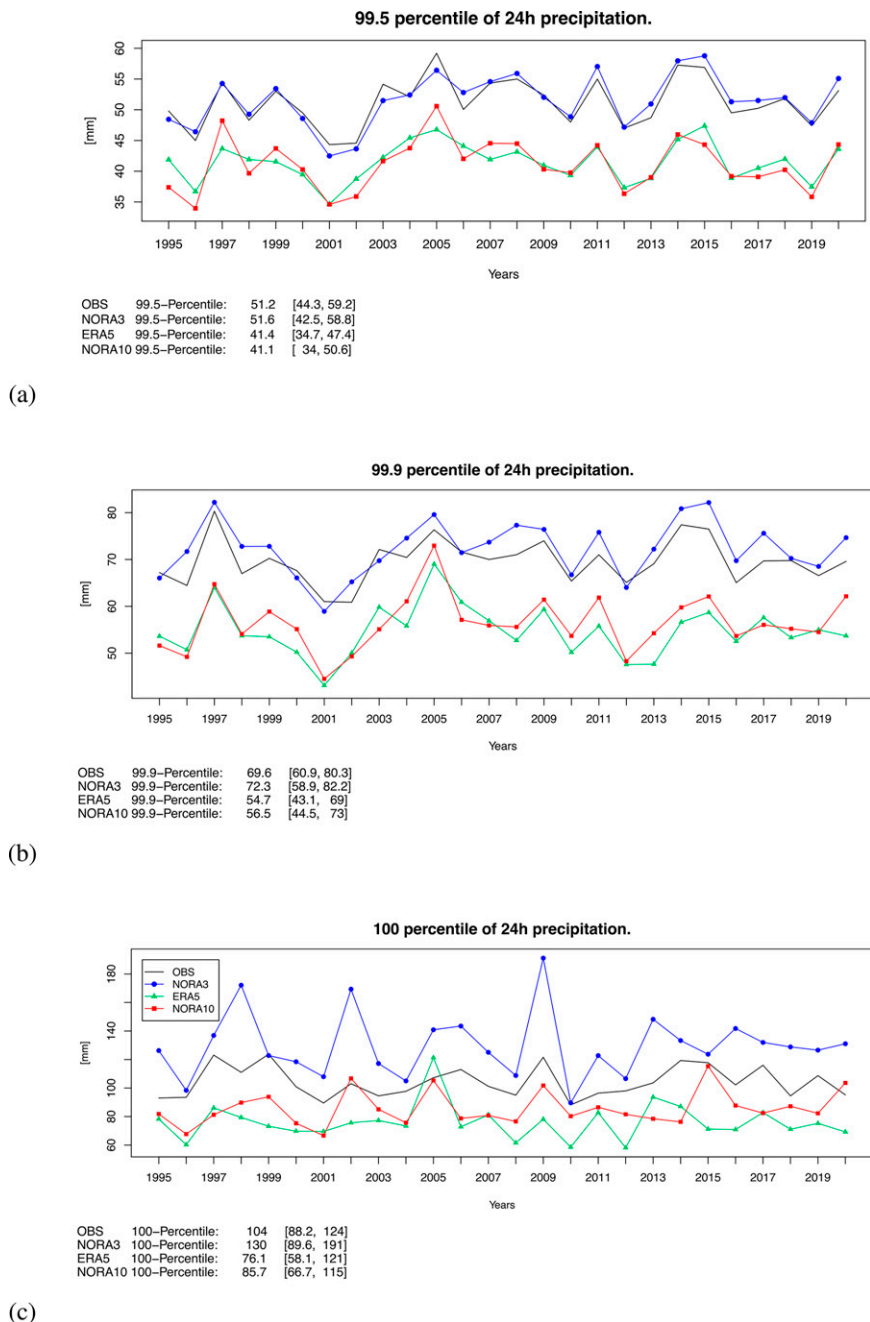


FIG. D1. Time series of the (a) 99.5th, (b) 99.9th, and (c) 100th percentile RR24H, with only wet days being used.

and GFS) had severe problems with the low temperatures in cases with temperature inversions. They related the problem to the initialization of the models and to a possible overestimation of the background turbulence in very stable conditions.

ERA5 also overestimates the lowest temperatures and does not go below  $-26^{\circ}\text{C}$  in Finnmark. The overestimation

of the 1st percentile in ERA5 is typically 4 K in Finnmark. However, ERA5 does also show a distinct underestimation of the 1st percentile T2m in large areas. The underestimation is particularly evident on the leeward side of the mountains. The same is also the case in the majority of the coastal areas. The underestimation of the 1st percentile in ERA5 was also seen in Fig. 7a.

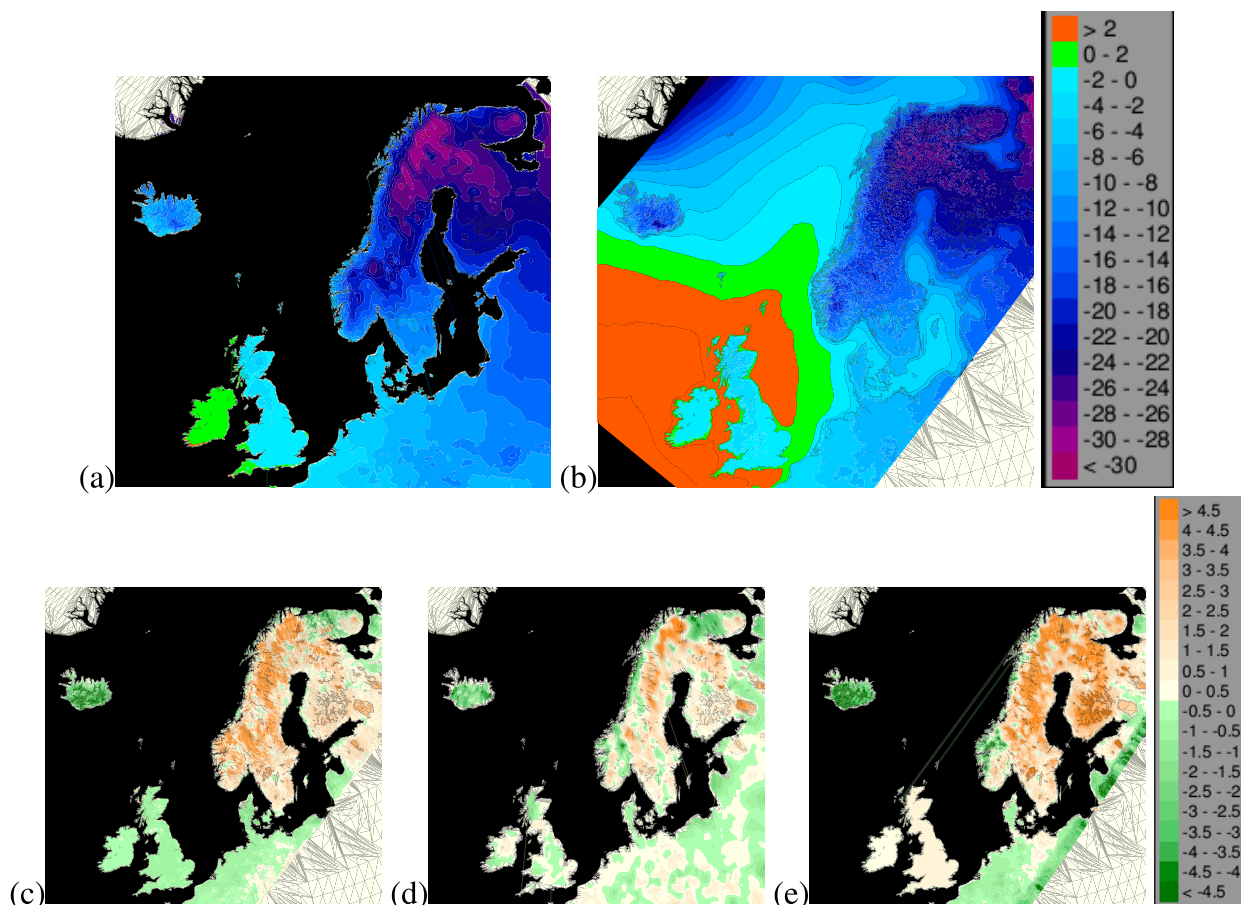


FIG. E1. (a) E-OBS and (b) NORA3 1st percentile of daily averaged T2m (°C). Also shown is the difference between (c) NORA3 and E-OBS, (d) between ERA5 and E-OBS, and (e) between NORA10 and E-OBS.

NORA10 is far too cold in the western part of Scandinavia and too warm farther east, away from the ocean. In Finnmark, NORA10 does not go below  $-25^{\circ}\text{C}$ .

The 99th-percentile 2-m temperature 99P-T2m varies from above  $20^{\circ}\text{C}$  near the southern coast of Norway to less than  $14^{\circ}\text{C}$  in the mountains and in some mountainous regions in northern Norway (see Fig. E2). The northeast part of the domain shows much higher temperatures for NORA3, ERA5, and NORA10 than what is found in E-OBS. We believe that this is partly explained by the lack of observations in the region, leading to an underestimation of the maximum temperature in E-OBS. NORA3 has a marginally higher 99P-T2m relative to E-OBS for the low-lying areas, and lower values than E-OBS in mountainous areas. NORA3 resolves the valleys much better than E-OBS, showing the higher temperatures stretching into the Langfjella area in central Norway.

ERA5 also exhibits a slightly higher 99P-T2m. The field is naturally smoother, missing the topographic details found in NORA3, but has only minor differences with E-OBS. NORA10 also shows 99P-T2m slightly higher than E-OBS. NORA10 does not represent lakes well, and 99P-T2m is

clearly underestimated over large inland water bodies (see, e.g., the Vänern and Vättern lakes in Sweden and the Ladoga and Onega Lakes in Russia).

The reason why ERA5 and NORA10 are biased high (positively) here while they are biased low in Fig. 7d can partly be explained by the missing coastal zone in E-OBS. ERA5 and NORA10 are most likely underestimating the 99th percentile in the coastal zone. This is in agreement with Fig. 5. There is also a marked uncertainty in the E-OBS data itself, as documented by Hofstra et al. (2009) who also found that E-OBS yields a small positive bias over large areas for 2-m temperature, consistent with our findings.

We have also looked at the daily accumulated rainfall RR24, but we find that the E-OBS data are biased low. This is in agreement with the findings of Hofstra et al. (2009) who remarked that E-OBS tends to be oversmoothed relative to the high-density datasets. Hofstra et al. (2009) also found that the E-OBS dataset is in better agreement with mean values than with extremes, with differences being much larger for precipitation than for temperature. They conclude that

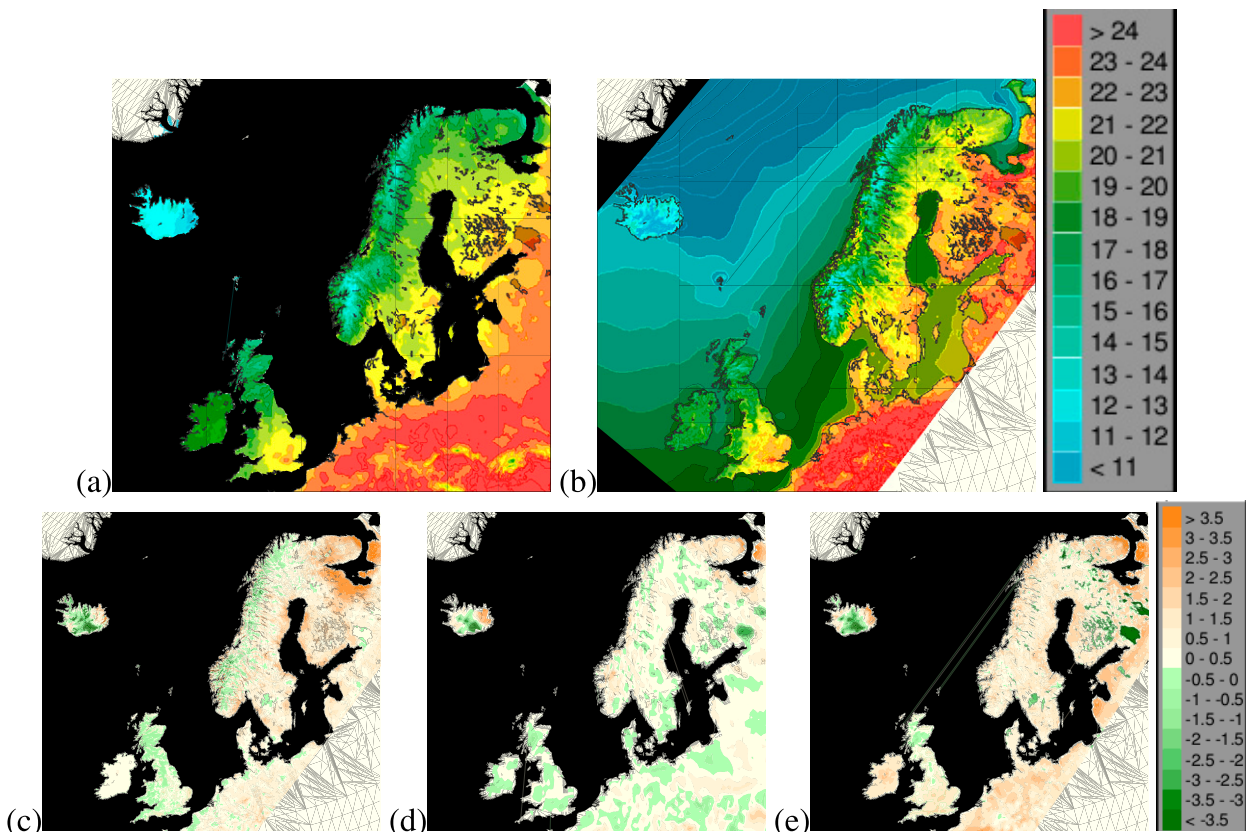


FIG. E2. As in Fig. E1, but for the 99th percentile.

the dataset should be used with caution in comparison with regional climate models and, in particular, when evaluating modeled precipitation extremes.

#### REFERENCES

- Aarnes, O. J., Ø. Breivik, and M. Reistad, 2012: Wave extremes in the northeast Atlantic. *J. Climate*, **25**, 1529–1543, <https://doi.org/10.1175/JCLI-D-11-00132.1>.
- Atlaskin, E., and T. Vihma, 2012: Evaluation of NWP results for wintertime nocturnal boundary-layer temperatures over Europe and Finland. *Quart. J. Roy. Meteor. Soc.*, **138**, 1440–1451, <https://doi.org/10.1002/qj.1885>.
- Avissar, R., and R. A. Pielke, 1989: A parameterization of heterogeneous land surfaces for atmospheric numerical models and its impact on regional meteorology. *Mon. Wea. Rev.*, **117**, 2113–2136, [https://doi.org/10.1175/1520-0493\(1989\)117<2113:APOHLS>2.0.CO;2](https://doi.org/10.1175/1520-0493(1989)117<2113:APOHLS>2.0.CO;2).
- Balsamo, G., P. Viterbo, A. Beljaars, B. van den Hurk, M. Hirschi, A. K. Betts, and K. Scipal, 2009: A revised hydrology for the ECMWF model: Verification from field site to terrestrial water storage and impact in the Integrated Forecast System. *J. Hydrometeorol.*, **10**, 623–643, <https://doi.org/10.1175/2008JHM1068.1>.
- Batrak, Y., and M. Müller, 2018: Atmospheric response to kilometer-scale changes in sea ice concentration within the marginal ice zone. *Geophys. Res. Lett.*, **45**, 6702–6709, <https://doi.org/10.1029/2018GL078295>.
- Bechtold, P., N. Semane, P. Lopez, J.-P. Chaboureau, A. Beljaars, and N. Bormann, 2014: Representing equilibrium and non-equilibrium convection in large-scale models. *J. Atmos. Sci.*, **71**, 734–753, <https://doi.org/10.1175/JAS-D-13-0163.1>.
- Bell, B., and Coauthors, 2020: Satellite observations in support of the Copernicus Climate Change Service. *Proc. SPIE*, 11527, 115270C, <https://doi.org/10.1117/12.2576497>.
- Bénard, P., J. Vivoda, J. Mašek, P. Smolíková, K. Yessad, C. Smith, R. Brožková, and J.-F. Geleyn, 2010: Dynamical kernel of the Aladin–NH spectral limited-area model: Revised formulation and sensitivity experiments. *Quart. J. Roy. Meteor. Soc.*, **136A**, 155–169, <https://doi.org/10.1002/qj.522>.
- Bengtsson, L., and Coauthors, 2017: The HARMONIE–AROME model configuration in the ALADIN–HIRLAM NWP system. *Mon. Wea. Rev.*, **145**, 1919–1935, <https://doi.org/10.1175/MWR-D-16-0417.1>.
- Boone, A., J. C. Calvet, and J. Noilhan, 1999: Inclusion of a third soil layer in a land surface scheme using the force-restore method. *J. Appl. Meteor.*, **38**, 1611–1630, [https://doi.org/10.1175/1520-0450\(1999\)038<1611:IOATSL>2.0.CO;2](https://doi.org/10.1175/1520-0450(1999)038<1611:IOATSL>2.0.CO;2).
- Bringfelt, B., M. Heikinheimo, N. Gustafsson, V. Perov, and A. Lindroth, 1999: A new land surface treatment for HIRLAM—Comparisons with NOPEX measurements. *J. Agric. For. Meteorol.*, **98–99**, 239–256, [https://doi.org/10.1016/S0168-1923\(99\)00101-X](https://doi.org/10.1016/S0168-1923(99)00101-X).

- Brousseau, P., Y. Seity, D. Ricard, and J. Léger, 2016: Improvement of the forecast of convective activity from the AROME-France system. *Quart. J. Roy. Meteor. Soc.*, **142**, 2231–2243, <https://doi.org/10.1002/qj.2822>.
- Bubnová, R., G. Hello, P. Bénard, and J.-F. Geleyn, 1995: Integration of the fully elastic equations cast in the hydrostatic pressure terrain-following coordinate in the framework of the ARPEGE/Aladin NWP system. *Mon. Wea. Rev.*, **123**, 515–535, [https://doi.org/10.1175/1520-0493\(1995\)123<0515:IOTFEE>2.0.CO;2](https://doi.org/10.1175/1520-0493(1995)123<0515:IOTFEE>2.0.CO;2).
- Cornes, R. C., G. van der Schrier, E. J. van den Besselaar, and P. D. Jones, 2018: An ensemble version of the E-OBS temperature and precipitation datasets. *J. Geophys. Res. Atmos.*, **123**, 9391–9409, <https://doi.org/10.1029/2017JD028200>.
- Cuxart, J., P. Bougeault, and J. L. Redelsberger, 2000: A turbulence scheme allowing for mesoscale and large-eddy simulations. *Quart. J. Roy. Meteor. Soc.*, **126**, 1–30, <https://doi.org/10.1002/qj.49712656202>.
- Daley, R., 1991: *Atmospheric Data Analysis*. Vol. 2, Atmospheric and Space Science Series. Cambridge University Press, 460 pp.
- Danielson, J., and D. Gesch, 2011: Global Multi-resolution Terrain Elevation Data 2010. USGS Tech. Rep. 2011-1073, 26 pp., <https://pubs.usgs.gov/of/2011/1073/pdf/of2011-1073.pdf>.
- Dee, D., and Coauthors, 2011: The ERA-Interim reanalysis: Configuration and performance of the data assimilation system. *Quart. J. Roy. Meteor. Soc.*, **137**, 553–597, <https://doi.org/10.1002/qj.828>.
- de Rooy, W. C., and A. P. Siebesma, 2010: Analytical expressions for entrainment and detrainment in cumulus convection. *Quart. J. Roy. Meteor. Soc.*, **136**, 1216–1227, <https://doi.org/10.1002/qj.640>.
- de Rosnay, P., G. Balsamo, C. Albergel, J. Muñoz-Sabater, and L. Isaksen, 2014: Initialisation of land surface variables for numerical weather prediction. *Surv. Geophys.*, **35**, 607–621, <https://doi.org/10.1007/s10712-012-9207-x>.
- Diamantakis, M., and L. Magnusson, 2016: Sensitivity of the ECMWF model to semi-Lagrangian departure point iterations. *Mon. Wea. Rev.*, **144**, 3233–3250, <https://doi.org/10.1175/MWR-D-15-0432.1>.
- Dörenkämper, M., and Coauthors, 2020: The making of the New European Wind Atlas—Part 2: Production and evaluation. *Geosci. Model Dev.*, **13**, 5079–5102, <https://doi.org/10.5194/gmd-13-5079-2020>.
- Douville, H., J.-F. Royer, and J.-F. Mahfouf, 1995: A new snow parameterization for the French community climate model. Part I: Validation in stand-alone experiments. *Climate Dyn.*, **12**, 21–35, <https://doi.org/10.1007/BF00208760>.
- ECMWF, 1989: ECMWF forecast model: Physical parameterization. ECMWF Research Manual 3, 154 pp., [http://cedadocs.ceda.ac.uk/1103/1/Research\\_manual\\_3\\_-\\_ECMWF\\_forecast\\_model\\_Physical\\_parameterization.pdf](http://cedadocs.ceda.ac.uk/1103/1/Research_manual_3_-_ECMWF_forecast_model_Physical_parameterization.pdf).
- Faroux, S., A. T. K. Tchuente, J. L. Roujean, V. Masson, E. Martin, and P. Le Moigne, 2013: ECOCLIMAP-II/Europe: A two-fold database of ecosystems and surface parameters at 1 km resolution based on satellite information for use in land surface, meteorological and climate models. *Geosci. Model Dev.*, **6**, 563–582, <https://doi.org/10.5194/gmd-6-563-2013>.
- Forbes, R. M., A. M. Tompkins, and A. Untch, 2011: A new prognostic bulk microphysics scheme for the IFS. ECMWF Tech. Memo. 649, 28 pp., <https://doi.org/10.21957/bf6vjvxx>.
- Førland, E. J., and I. Hanssen-Bauer, 2000: Increased precipitation in the Norwegian Arctic: True or false? *Climatic Change*, **46**, 485–509, <https://doi.org/10.1023/A:1005613304674>.
- , K. Isaksen, J. Lutz, I. Hanssen-Bauer, T. V. Schuler, A. Dobler, H. M. Gjelten, and D. Vikhamar-Schuler, 2020: Measured and modeled historical precipitation trends for Svalbard. *J. Hydrometeorol.*, **21**, 1279–1296, <https://doi.org/10.1175/JHM-D-19-0252.1>.
- Furevik, B. R., and H. Haakenstad, 2012: Near-surface marine wind profiles from rawinsonde and NORA10 hindcast. *J. Geophys. Res.*, **117**, D23106, <https://doi.org/10.1029/2012JD018523>.
- Gandin, L. S., and A. H. Murphy, 1992: Equitable skill scores for categorical forecasts. *Mon. Wea. Rev.*, **120**, 361–370, [https://doi.org/10.1175/1520-0493\(1992\)120<0361:ESSFCF>2.0.CO;2](https://doi.org/10.1175/1520-0493(1992)120<0361:ESSFCF>2.0.CO;2).
- Haakenstad, H., Ø. Breivik, M. Reistad, and O. J. Aarnes, 2020: NORA10EI: A revised regional atmosphere-wave hindcast for the North Sea, the Norwegian Sea and the Barents Sea. *Int. J. Climatol.*, **40**, 4347–4373, <https://doi.org/10.1002/joc.6458>.
- , —, B. R. Furevik, M. Reistad, P. Bohlinger, and O. J. Aarnes, 2021: NORA3: A nonhydrostatic high-resolution hindcast of the North Sea, the Norwegian Sea, and the Barents Sea. *J. Appl. Meteor. Climatol.*, **60**, 1443–1464, <https://doi.org/10.1175/JAMC-D-21-0029.1>.
- Haarsma, R. J., W. Hazeleger, C. Severijns, H. de Vries, A. Sterl, R. Bintanja, G. J. van Oldenborgh, and H. W. van den Brink, 2013: More hurricanes to hit western Europe due to global warming. *Geophys. Res. Lett.*, **40**, 1783–1788, <https://doi.org/10.1002/grl.50360>.
- Habets, F., and Coauthors, 1999: The ISBA surface scheme in a macroscale hydrological model applied to the Hapex-Mobilhy area: Part I: Model and database. *J. Hydrol.*, **217**, 75–96, [https://doi.org/10.1016/S0022-1694\(99\)00019-0](https://doi.org/10.1016/S0022-1694(99)00019-0).
- Hanssen-Bauer, I., and P. Nordli, 1998: Annual and seasonal temperature variations in Norway 1976–1997. Norwegian Meteorological Institute Tech. Rep. 25/98, 29 pp., [https://www.met.no/publikasjoner/met-report/met-report-1998/\\_attachment/download/42d2421c-e874-4043-abf9-798fd5be61d3:a4957c7c7a30ce24f5502ea172c621b65e6ee96f/MET-report-25-1998.pdf](https://www.met.no/publikasjoner/met-report/met-report-1998/_attachment/download/42d2421c-e874-4043-abf9-798fd5be61d3:a4957c7c7a30ce24f5502ea172c621b65e6ee96f/MET-report-25-1998.pdf).
- Hersbach, H., and Coauthors, 2020: The ERA5 global reanalysis. *Quart. J. Roy. Meteor. Soc.*, **146**, 1999–2049, <https://doi.org/10.1002/qj.3803>.
- Hirahara, S., M. A. Balmaseda, E. de Boisson, and H. Hersbach, 2016: Sea surface temperature and sea ice concentration for ERA5. ERA Rep. Series 26, 25 pp., <https://www.ecmwf.int/node/16555>.
- Hofstra, N., M. Haylock, M. New, and P. D. Jones, 2009: Testing E-OBS high-resolution gridded data set of daily precipitation and surface temperature. *J. Geophys. Res.*, **114**, D21101, <https://doi.org/10.1029/2009JD011799>.
- Horányi, A., 2017: Some aspects on the use and impact of observations in the ERA5 Copernicus Climate Change Service reanalysis. *Idojaras*, **121**, 329–344.
- Iacono, M., J. Delamere, E. Mlawer, M. Shephard, S. Clough, and W. Collins, 2008: Radiative forcing by long-lived greenhouse gases: Calculations with the AER radiative transfer models. *J. Geophys. Res.*, **113**, D13103, <https://doi.org/10.1029/2008JD009944>.
- IPCC, 2007: *Climate Change 2007: The Physical Science Basis*. Cambridge University Press, 996 pp., [https://www.ipcc.ch/site/assets/uploads/2018/05/ar4\\_wg1\\_full\\_report-1.pdf](https://www.ipcc.ch/site/assets/uploads/2018/05/ar4_wg1_full_report-1.pdf).

- Khairoutdinov, M., and Y. Kogan, 2000: A new cloud physics parameterization in a large-eddy simulation model of marine stratocumulus. *Mon. Wea. Rev.*, **128**, 229–243, [https://doi.org/10.1175/1520-0493\(2000\)128<0229:ANCPPI>2.0.CO;2](https://doi.org/10.1175/1520-0493(2000)128<0229:ANCPPI>2.0.CO;2).
- Kjelland, G., 2005: KVALOBS—The quality assurance system of Norwegian Meteorological Institute observations. *WMO Technical Conf. on Meteorological and Environmental Instruments and Methods of Observation*, Bucharest, Romania, WMO, 3(13), [https://library.wmo.int/doc\\_num.php?explnum\\_id=9293](https://library.wmo.int/doc_num.php?explnum_id=9293).
- Køltzow, M., B. Casati, E. Bazile, T. Haiden, and T. Valkonen, 2019: An NWP model intercomparison of surface weather parameters in the European Arctic during the Year of Polar Prediction special observing period Northern Hemisphere I. *Wea. Forecasting*, **34**, 2279–2292, <https://doi.org/10.1175/WAF-D-19-0003.1>.
- , —, T. Haiden, and T. Valkonen, 2020: Verification of solid precipitation forecasts from numerical weather prediction models in Norway. *Wea. Forecasting*, **35**, 959–983, <https://doi.org/10.1175/WAF-D-20-0060.1>.
- , H. Schyberg, E. Støylen, and X. Yang, 2022: Value of the Copernicus Arctic Regional ReAnalysis (CARRA) in representing near-surface temperature and wind speed in the north-east European Arctic. *Polar Res.*, **41**, <https://doi.org/10.33265/polar.v41.8002>.
- Kuo, H. L., 1974: Further studies of the parameterization of the influence of cumulus convection on large-scale flow. *J. Atmos. Sci.*, **31**, 1232–1240, [https://doi.org/10.1175/1520-0469\(1974\)031<1232:FSOTPO>2.0.CO;2](https://doi.org/10.1175/1520-0469(1974)031<1232:FSOTPO>2.0.CO;2).
- Lascaux, F., E. Richard, and J.-P. Pinty, 2006: Numerical simulations of three different MAP IOPs and the associated microphysical processes. *Quart. J. Roy. Meteor. Soc.*, **132**, 1907–1926, <https://doi.org/10.1256/qj.05.197>.
- Le Moigne, P., Ed., 2012: SURFEX v7.2 scientific documentation. CNRM/GAME Météo-France/CNRS Doc., 237 pp., <https://gmd.copernicus.org/articles/6/929/2013/gmd-6-929-2013-supplement.pdf>.
- Lenderink, G., and A. A. Holtslag, 2004: An updated length-scale formulation for turbulent mixing in clear and cloudy boundary layers. *Quart. J. Roy. Meteor. Soc.*, **130**, 3405–3427, <https://doi.org/10.1256/qj.03.117>.
- Manners, J., S. B. Vosper, and N. Roberts, 2012: Radiative transfer over resolved topographic features for high-resolution weather prediction. *Quart. J. Roy. Meteor. Soc.*, **138**, 720–733, <https://doi.org/10.1002/qj.956>.
- Masson, V., and Coauthors, 2013: The SURFEXv7.2 land and ocean surface platform for coupled or offline simulation of earth surface variables and fluxes. *Geosci. Model Dev.*, **6**, 929–960, <https://doi.org/10.5194/gmd-6-929-2013>.
- Mlawer, E. J., S. J. Taubman, P. D. Brown, M. J. Iacono, and S. A. Clough, 1997: Radiative transfer for inhomogeneous atmospheres: RRTM, a validated correlated-*k* model for the longwave. *J. Geophys. Res.*, **102D**, 16663–16682, <https://doi.org/10.1029/97JD00237>.
- Müller, M., Y. Batrak, J. Kristiansen, M. A. Ø. Køltzow, G. Noer, and A. Korosov, 2017a: Characteristics of a convective-scale weather forecasting system for the European Arctic. *Mon. Wea. Rev.*, **145**, 4771–4787, <https://doi.org/10.1175/MWR-D-17-0194.1>.
- , and Coauthors, 2017b: AROME-MetCoOp: A Nordic convective-scale operational weather prediction model. *Wea. Forecasting*, **32**, 609–627, <https://doi.org/10.1175/WAF-D-16-0099.1>.
- Pinty, J.-P., and P. Jabouille, 1998: A mixed-phase cloud parameterization for use in a mesoscale non-hydrostatic model: Simulation of a squall line and of orographic precipitation. Preprints, *Conf. on Cloud Physics*, Everett, WA, Amer. Meteor. Soc., 217–220.
- Rasmussen, R., and Coauthors, 2012: How well are we measuring snow? The NOAA/FAA/NCAR winter precipitation test bed. *Bull. Amer. Meteor. Soc.*, **93**, 811–829, <https://doi.org/10.1175/BAMS-D-11-00052.1>.
- Reistad, M., Ø. Breivik, H. Haakenstad, O. Aarnes, and B. Furevik, 2009: A high-resolution hindcast of wind and waves for the North Sea, the Norwegian Sea and the Barents Sea. Norwegian Meteorological Institute Research Rep. 14/2009, 76 pp.
- , —, —, —, —, and J.-R. Bidlot, 2011: A high-resolution hindcast of wind and waves for the North Sea, the Norwegian Sea, and the Barents Sea. *J. Geophys. Res.*, **116**, C05019, <https://doi.org/10.1029/2010JC006402>.
- Samuelsson, P., M. Homleid, T. Aspelien, and U. Andrae, 2018: Two patches in cy40h HARMONIE-AROME and modified tree height and snow roughness length for the MetCoOp domain. *ALADIN-HIRLAM Newsletter*, No. 10, SMHI and MetNorway, 107–115, <https://www.umr-cnrm.fr/aladin/IMG/pdf/nl10.pdf>.
- Savijärvi, H., 1990: Fast radiation parameterization schemes for mesoscale and short-range forecast models. *J. Appl. Meteor.*, **29**, 437–447, [https://doi.org/10.1175/1520-0450\(1990\)029<0437:FRPSFM>2.0.CO;2](https://doi.org/10.1175/1520-0450(1990)029<0437:FRPSFM>2.0.CO;2).
- Schaller, N., and Coauthors, 2020: The role of spatial and temporal model resolution in a flood event storyline approach in western Norway. *Wea. Climate Extremes*, **29**, 100259, <https://doi.org/10.1016/j.wace.2020.100259>.
- Seity, Y., P. Brousseau, S. Malardel, G. Hello, P. Benard, F. Bouttier, C. Lac, and V. Masson, 2011: The AROME-France convective-scale operational model. *Mon. Wea. Rev.*, **139**, 976–991, <https://doi.org/10.1175/2010MWR3425.1>.
- Senkova, A. V., L. Rontu, and H. Savijärvi, 2007: Parameterization of orographic effects on surface radiation in HIRLAM. *Tellus*, **59**, 279–291, <https://doi.org/10.1111/j.1600-0870.2007.00235.x>.
- Siebesma, A. P., and Coauthors, 2003: A large eddy simulation intercomparison study of shallow cumulus convection. *J. Atmos. Sci.*, **60**, 1201–1219, [https://doi.org/10.1175/1520-0469\(2003\)60<1201:ALESIS>2.0.CO;2](https://doi.org/10.1175/1520-0469(2003)60<1201:ALESIS>2.0.CO;2).
- , P. M. Soares, and J. Teixeira, 2007: A combined eddy-diffusivity mass-flux approach for the convective boundary layer. *J. Atmos. Sci.*, **64**, 1230–1248, <https://doi.org/10.1175/JAS3888.1>.
- Soares, P., P. Miranda, A. Siebesma, and J. Teixeira, 2004: An eddy-diffusivity mass-flux parameterization for dry and shallow cumulus convection. *Quart. J. Roy. Meteor. Soc.*, **130**, 3365–3383, <https://doi.org/10.1256/qj.03.223>.
- Solbrekke, I. M., A. Sorteberg, and H. Haakenstad, 2021: The 3 km Norwegian reanalysis (NORA3)—A validation of offshore wind resources in the North Sea and the Norwegian Sea. *Wind Energy Sci.*, **6**, 1501–1519, <https://doi.org/10.5194/wes-6-1501-2021>.
- Sundqvist, H., 1993: Inclusion of ice phase of hydrometeors in cloud parameterization for mesoscale and largescale models. *Contrib. Atmos. Phys.*, **66**, 137–147.
- Termonia, P., and Coauthors, 2018: The ALADIN System and its canonical model configurations AROME CY41T1 and

- ALARO CY40T1. *Geosci. Model Dev.*, **11**, 257–281, <https://doi.org/10.5194/gmd-11-257-2018>.
- Uden, P., and Coauthors, 2002: HIRLAM-5 scientific documentation. SMHI Tech. Rep. GKSS 97/E/46, 144 pp., [https://repositorio.aemet.es/bitstream/20.500.11765/6323/1/HIRLAMSciDoc\\_Dec2002.pdf](https://repositorio.aemet.es/bitstream/20.500.11765/6323/1/HIRLAMSciDoc_Dec2002.pdf).
- van Meijgaard, E., L. H. van Ulft, G. Lenderink, S. D. Roode, E. L. Wipler, R. Boers, and R. van Timmermans, 2012: Refinement and application of a regional atmospheric model for climate scenario calculations of western Europe. KVR Research Rep. 054/12, 44 pp.
- Vihma, T., and Coauthors, 2015: The atmospheric role in the Arctic water cycle: A review on processes, past and future changes and their impacts. *J. Geophys. Res. Biogeosci.*, **121**, 586–620, <https://doi.org/10.1002/2015JG003132>.
- Weisse, R., and H. Günther, 2007: Wave climate and long-term changes for the southern North Sea obtained from a high-resolution hindcast 1958–2002. *Ocean Dyn.*, **57**, 161–172, <https://doi.org/10.1007/s10236-006-0094-x>.
- Whan, K., J. Sillmann, N. Schaller, and R. Haarsma, 2020: Future changes in atmospheric rivers and extreme precipitation in Norway. *Climate Dyn.*, **54**, 2071–2084, <https://doi.org/10.1007/s00382-019-05099-z>.
- Wilks, D. S., 2006: *Statistical Methods in the Atmospheric Sciences*. 2nd ed. Academic Press, 627 pp.
- Wolff, M. A., K. Isaksen, A. Petersen-Øverleir, K. Ødemark, T. Reitan, and R. Brækkan, 2015: Derivation of a new continuous adjustment function for correcting wind-induced loss of solid precipitation: Results of a Norwegian field study. *Hydrol. Earth Syst. Sci.*, **19**, 951–967, <https://doi.org/10.5194/hess-19-951-2015>.
- Yang, X., 2005: Background blending using an incremental spatial filter. *HIRLAM Newsletter*, No. 49, HIRLAM Consortium, 3–11.
- , and Coauthors, 2020: C3S Arctic regional reanalysis—Full system documentation. Copernicus Climate Change Service Tech. Doc., 63 pp., <https://datastore.copernicus-climate.eu/documents/reanalysis-carra/CARRAFullSystemDocumentationFinal.pdf>.